Remote sensing of cyanobacteria-dominant algal blooms and water quality parameters in Zeekoevlei, a small hypertrophic lake, using MERIS

Mark W. Matthews[a,*], Stewart Bernard[bc], Kevin Winter[a]

[a] *Department of Environmental and Geographical Science, University of Cape Town, Rondebosch, 7700, South Africa*
[b] *Department of Oceanography, University of Cape Town, Rondebosch, 7700, South Africa*
[c] *Ecosystems Earth Observation, Council for Scientific and Industrial Research, 11 Jan Cilliers St, Stellenbosch, South Africa*

Abstract

Eutrophication and cyanobacterial algal blooms present an increasing threat to the health of freshwater ecosystems and to humans who use these resources for drinking and recreation. Remote sensing is being used increasingly as a tool for monitoring these phenomena in inland and near-coastal waters. This study uses the Medium Resolution Imaging Spectrometer (MERIS) to view Zeekoevlei, a small hypertrophic freshwater lake situated on the Cape Flats in Cape Town, South Africa, dominated by *Microcystis* cyanobacteria. The lake's small size, highly turbid water, and covariant water constituents present a challenging case for both algorithm development and atmospheric correction. The objectives of the study are to assess the optical properties of the lake, to evaluate various atmospheric correction procedures, and to compare the performance of empirical and semi-analytical algorithms in hypertrophic water. *In situ* water quality parameter and radiometric measurements were made simultaneous to MERIS overpasses. Upwelling radiance measurements at depth 0.66m were corrected for instrument self-shading and processed to the water-leaving reflectance using downwelling irradiance measurements and estimates of the vertical attenuation coefficient for upward radiance, K_u, generated from a simple bio-optical model estimating the total absorption, $a(\lambda)$, and backscattering coefficients, $b_b(\lambda)$. The normalized water-leaving reflectance was used for assessing the accuracy of image-based Dark Object Subtraction and 6S Radiative Transfer Code atmospheric correction procedures applied to MERIS. Empirical algorithms for estimating chorophyll *a* (Chl *a*), Total Suspended Solids (TSS), Secchi Disk depth (SD) and absorption by CDOM (a_{CDOM}) were derived from simultaneously collected *in situ* and MERIS measurements. The empirical algorithms gave high correlation coefficient values, although have a limited ability to separate between signals from covariant water constituents. The MERIS Neural Network algorithms utilized in the standard Level 2 Case 2 waters product and Eutrophic Lakes processor were also used to derive water constituent concentrations. However, these failed to produce reasonable comparisons with *in situ* measurements owing to the failure of atmospheric correction and divergence between the optical properties and ranges used to train the algorithms and those of Zeekoevlei. Maps produced using the empirical algorithms effectively show the spatial and temporal variability of the water quality parameters during April 2008. On the basis of the results it is argued that MERIS is the current optimal sensor for frequent change detection applications in inland waters. This study also demonstrates the considerable potential value for simple TOA algorithms for hypertrophic systems. It is recommended that regional algorithm development be prioritized in southern Africa and that remote sensing be integrated into future operational water quality monitoring systems.

***Keywords*: Remote sensing; MERIS; Water quality; Cyanobacterial algal blooms; Freshwater resources; Zeekoevlei; Monitoring; Empirical algorithms; Eutrophic Lakes Processor; NN algorithms; South Africa.**

[*] Corresponding author. Tel.: +27834564506; Fax.: +27866448708; E-mail: mark.matthews@uct.ac.za

1. Introduction

Anthropogenic modification has severely deteriorated the quality of the world's limited freshwater resources and the impact from eutrophication is likely to become even more severe in developing countries in this century (Brönmark & Hansson, 2002). There is evidence to suggest that eutrophic conditions lead to increasing dominance of cyanobacterial species of algae which may pose a serious threat to lake ecosystems, and even animals and humans, through the production of potentially lethal cyanotoxins (Downing et al., 2001, Falconer, 2001). Recent findings show that global climate change and higher temperatures are expected to worsen the shift to turbid-water, cyanobacteria-dominated conditions in lakes (Mooij et al., 2007, see Johnk et al., 2008). In South Africa eutrophic conditions already exist in approximately one in every five major impoundments and in 18 out of 25 major river catchments (DWAF, 2003, de Villiers & Thiart, 2007). The cyanophyta *Microcysitis aeruginosa* which produces *microcystin* toxin is widespread in southern Africa and has been found responsible for numerous animal deaths (Scott, 1991, Oberholster et al., 2005). In order to increase knowledge of water quality, and the occurrence and extent of eutrophication and cyanobacterial blooms, satellite remote sensing is being used increasingly as a tool for monitoring these phenomena in inland and near-coastal waters. Commonly detected parameters include the concentrations of phytoplankton pigments chlorophyll *a* (Chl *a*) and phycocyanin (the accessory pigment present in cyanobacteria) (Simis et al., 2005, Kutser et al., 2006, Moses et al., 2009b); the concentrations of Total Suspended Solids (TSS) and Inorganic Suspended Solids (ISS) (Onderka & Pekarova, 2008); indicators of water clarity such as turbidity and Secchi disk depth (SD) (Giardino et al., 2001, Chen et al., 2007); and absorption by Coloured Dissolved Organic Matter (CDOM)(Kutser et al., 2005). The Medium Resolution Imaging Spectrometer (MERIS) onboard ESA's Envisat is particularly well suited to these applications (Giardino et al., 2005, Odermatt et al., 2008, Moses et al., 2009a). In Full Resolution mode MERIS acquires images with a pixel width of approximately 260 by 300 m every two to three days in 15 spectral bands ideally positioned for water, land and atmospheric correction applications. While MERIS is poorly suited to viewing lakes smaller than about 1 km^2 which make up the great majority of the world's 304 million estimated lakes, its resolution is probably sufficient to view the remaining estimated 57% of the total surface area of the world's lakes (Downing et al., 2006). The high signal-to-noise ratio is designed for viewing water targets that have a very small signal relative to land. Furthermore, the free availability of MERIS data from ESA via CD and DVD format make it a viable option for use in the developing world where data cost and availability, and slow and intermittent internet connectivity, can be a considerable hindrance to remote sensing applications. This paper presents preliminary findings from MERIS for Zeekoevlei lake which is situated on the Cape Flats, Cape Town, South Africa. Zeekoevlei is an archetype of a severely degraded hypertrophic shallow turbid lake with near-permanent algal blooms dominated by cyanobacteria and is therefore well-suited for assessing remote sensing in these conditions (Harding, 1992).

The empirical approach of remote sensing uses experimental data sets and statistical regression techniques to generate empirical algorithms relating the water-leaving reflectances or radiances at the sensor in specific spectral bands or band ratios/combinations to *in situ* water quality parameter measurements (e.g. Moses et al., 2009a). The simplicity of the empirical approach means that it is easy to implement (especially in instances where *in situ* data is regularly collected) and that the algorithms are generally robust. However, as with most algorithms they are limited to the constraints of the data set from which they are derived (and are thus not usually applicable across seasons or areas), and may be unable to separate non-unique signals in instances where water constituents are covariant. More complex semi-analytical approaches use a variety of inversion techniques, either as in-water or coupled water-atmosphere algorithms (e.g. Odermatt et al., 2008). Semi-analytical algorithms typically retrieve IOPs such as the absorption coefficients of Coloured Dissolved Organic Matter (CDOM), detritus and phytoplankton, and the total and particulate backscattering coefficients (Lee et al., 2002). This approach maximises the information that can be gained from the remote sensing signal, allowing geophysical parameters, such as Chl *a* concentration, to be derived using known regional IOP parameterisations (e.g. Ciotti & Bricaud, 2006). There are also some examples of direct retrieval of Chl *a* and TSS using inversion procedures (e.g. Brando & Dekker, 2003, Kutser, 2004). Semi-analytical algorithms are well suited to operational water quality monitoring systems because they are able to operate independently of concurrent *in situ* measurements. They are also potentially more powerful in their ability to separate the signal of different in-water constituents by solving for several parameters simultaneously. However their use of many, if not all of the spectral bands available, makes them very sensitive to errors in the atmospheric correction and some algorithms require arduous training or re-parameterisation using regional IOP measurements. In this paper, MERIS scenes and *in situ* hyperspectral radiometric reflectance with concurrent *in situ* measurements are used to derive and assess a variety of empirical and semi-analytical algorithms for

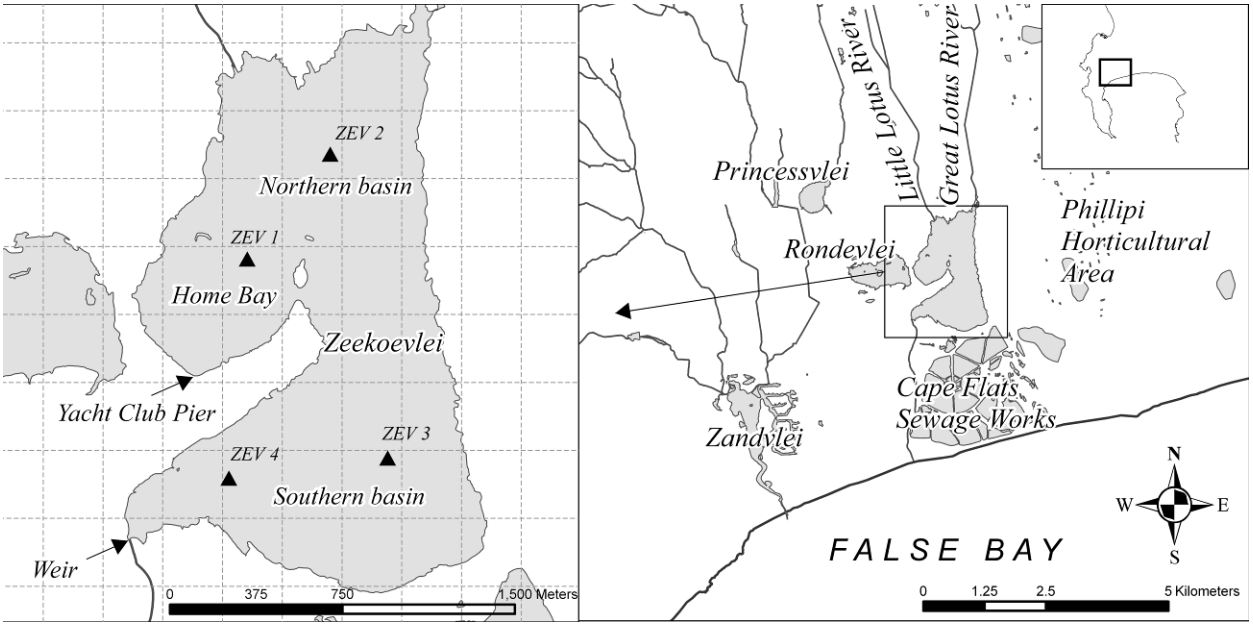

Fig. 1. Map showing Zeekoevlei on the Cape Flats with surrounding lakes and adjacent Cape Flats Sewage Works to the south (right). A grid shows the size of MERIS pixels and the four sample points are labelled ZEV 1 to ZEV 4 (left).

estimating parameters including Chl *a*, TSS, absorption by CDOM (a_{CDOM}) and SD. The MERIS Inverse Radiative Transfer Model Neural Network (IRTM-NN) semi-analytical algorithm from the standard Level 2 Product and Eutrophic Lakes processor (V. 1.0.2) in VISAT BEAM (V. 4.2) is tested and also used to estimate atmospheric properties. The advantages and constraints of using empirical versus semi-analytical algorithms in hypertrophic systems are considered using a comparison between algorithm estimates and *in situ* measurements.

Atmospheric correction forms a vital component of any remote sensing study as the great majority of the signal detected at the sensor over water is from the atmosphere. Over turbid waters scattering from suspended matter in the near infrared bands mean than typical corrections based on black pixel assumptions fail (Vidot & Santer, 2005) and alternative atmospheric correction schemes using Radiative transfer models or other approaches are needed (e.g. Guanter et al., 2009, Shi & Wang, 2009). In this paper, the performance of image-based and Radiative Transfer Code (6S) corrections are evaluated using *in situ* reflectance and Aerosol Optical Thickness (AOT) measurements. The Improve Contrast between Ocean and Land processor (ICOL) processor (Santer & Zagolski, 2008) for MERIS may be used to correct water pixels for the adjacency effect, which is known to be a significant source of error in the near-infrared bands of water adjacent to or near land (Giardino et al., 2007). However, the use of ICOL over small turbid lakes, such as Zeekoevlei, is problematic due to the inability of Version 1 of the processor to discriminate between land and water pixels, as described in this paper.. The aim of the paper is to provide an initial application and evaluation of procedures of water remote sensing in hypertrophic lake water. Within this aim there are three main objectives, namely to assess the lakes optical properties, to evaluate various atmospheric correction procedures over a very turbid water target, and to compare the performance of a variety of empirical and semi-analytical algorithms for estimating geophysical parameters. The study also contributes towards increasing understanding of the temporal and spatial dynamics of cyanobacteria-dominant blooms in Zeekoevlei with the aim of improving monitoring capabilities in hypertrophic waters. The findings of the study will be useful to future operational eutrophication and water quality monitoring systems based on remote sensing in southern Africa.

2. Site Description

Zeekoevlei, literally translated from Afrikaans meaning 'Hippo Lake', is a small freshwater lake situated on the Cape Flats, Cape Town, South Africa (Fig. 1). Zeekoevlei is the largest of a system of coastal lakes and lies adjacent to the Cape Flats Sewage Works to the south. The lake is roughly divided into three basins: the northern basin, near the inlets from the Great and Little Lotus Rivers; Home Bay, a sheltered corner in the north-east; and the southern basin, also known as Storm Bay (Fig. 1).

Table 1
Input data used in bio-optical simulations. Cross-sections for detritus and minerals are in units μm^2 and wavelength is in nm.

Component	Details	Reference
a_w	From Pope and Fry (1997) [400 to 715 nm] and Kou et al. (1993) [720 to 750 nm]	(Pegau et al., 2003)
a^*_ϕ	*Synechocystis* (generic marine cyanophyte) *Dunaliella Bioculata* (marine chlorophyte)	(Ahn et al., 1992)
a_{CDOM}	*In situ* measurements fitted to equation (2)	This study
a^*_d	$\sigma_{a,det} = 8.791\times10^{-4} \times \exp(-0.00847\lambda)$	(Stramski et al., 2001)
a^*_m	$\sigma_{a,min} = 1.013\times10^{-3} \times \exp(-0.00846\lambda)$	(Stramski et al., 2001)
b_w , b_{bw}	From Buiteveld et al. (1994) (b_{bw} = ½ b_w)	(Pegau et al., 2003)
b^*_ϕ , $b^*_{b\phi}$	*Synechocystis* (generic marine cyanophyte) *Dunaliella Bioculata* (marine chlorophyte)	(Ahn et al., 1992)
b^*_d	$\sigma_{b,det} = 0.1425\lambda^{-0.9445}$	(Stramski et al., 2001)
b^*_m	$\sigma_{b,min} = 0.7712\lambda^{-0.9764}$	(Stramski et al., 2001)
b^*_{bd}	$\sigma_{bb,det} = 5.881\times10^{-4}\lambda^{-0.8997}$	(Stramski et al., 2001)
b^*_{bm}	$\sigma_{bb,min} = 1.790\times10^{-2}\lambda^{-0.9140}$	(Stramski et al., 2001)

Zeekoevlei was proclaimed a local nature reserve in 2000 and is an important component of the City of Cape Town's Biodiversity Network and the False Bay Ecology Park. The lake is shallow with a mean depth of only 1.9m attributed to the large deposits of organically rich sediment (Harding, 1992). Water flowing into Zeekoevlei via the Lotus Rivers is very polluted and high in nutrient concentrations as a result of large areas of informal settlements and horticultural agriculture in the catchment (Grobicki et al., 2001). The primary source of nutrients, however, is from underground seepage from the Cape Flats Sewage Works (Southern Waters Ecological Research and Consulting, 2000). The mean concentrations of dissolved nutrients phosphorus (P) and nitrogen (N) measured by the City's Scientific Services from 1981 to 2008 is 0.819 and 3.37 $g.m^{-3}$, respectively, with a mean Chl *a* concentration of 235.1 $mg.m^{-3}$ and dry weight suspended solids concentration of 84.1 $g.m^{-3}$ (Matthews, 2009). Very high primary production levels are sustained by strong prevailing winds which cause continual mixing of the surface layer, such that the lake is 'hypermictic' and analogous to a continuous fermentor for phytoplankton growth (Harding, 1997). The phytoplankton assemblage has low species diversity and displays equilibrium between cyanophyte and chlorophyte species in terms of biomass; however in terms of cell counts the cyanobacterium *Microcystis aeruginosa* is by far the most dominant species, with cell counts from 4 000 to 7 000 000 $cells.m\ell^{-3}$ (Harding, 1992). In fact, Zeekoevlei has no fewer than five cyanobacterial species capable of producing toxins (*ibid.*), and in 1995 a dog was killed by *nodularin* poisoning (Harding et al., 1995). It is reasonable to assume that Zeekoevlei continues to remain a health hazard to animals and recreational users as water quality conditions do not appear to have improved over the last decade (Haskins, 2006). Zeekoevlei is a good site for testing and developing techniques for remote sensing in small, highly turbid, hypertrophic cyanobacteria-dominated freshwater lakes. The lake's small size, highly turbid water, and covariant water constituents present a challenging case for remote sensing both in terms of algorithm development and atmospheric correction.

3. Methods

3.1 In situ measurements and bio-optical model

In situ sampling of limnological and atmospheric properties and measurements of Inherent and Apparent Optical Properties (AOPs) were carried our simultaneous to MERIS overpasses during April 2008. A total of 31 water samples were collected from four sample points around the lake (see Fig. 1) between 9 and 12 am local time usually within an hour of MERIS overpasses on clear or partially cloudy days (not all sample points were always sampled). Samples were kept cool during transportation to the laboratory and analysed within three to four hours after collection. All analyses were carried out in triplicate using the mean as the final value. Phytoplankton pigments (Chl *a*) were initially extracted by filtering 20 ml of sample through Whatmann GF/F filters and grinding the filter paper submerged in 9 ml of 90% acetone with a glass rod for one minute. After extraction for 24 hours in a freezer, the test tubes were centrifuged at 2500rpm for 5 minutes, transferred to glass tubes, and read in a Turner Designs 10-AU Fluorometer (Holm-Hansen et al., 1965). The samples were corrected for absorption by pheophytin pigments. However the Chl *a* values were anomalously low compared to historical measurements most probably due to the poor extraction efficiency of acetone with phytoplankton assemblages dominated by cyanobacteria, as noted by other authors (Robarts & Zohary, 1984, see Pápista et al., 2002). Spectrophotometric analysis of nine samples in 95% ethanol using a Shimadzu UV-2501 spectrophotometer (Sartory & Grobbelaar, 1984) gave Chl *a* values 64% higher than those concurrently measured in acetone. The filter papers were ground with a glass rod for 1 minute and the supernatant heated in an oven set to 80° C for 5

minutes before extraction in a freezer for 24 hours. The path length of the quartz cuvettes was 1cm and the samples ware acidified to correct for absorption by pheophytin pigments. The previously measured fluorometric Chl *a* readings were corrected by multiplying by the average correction factor for the test (= 1.64) assuming the phytoplankton assemblage was constant over the sampling period, which is reasonable given the spectrally invariant shapes of the water leaving radiance (see Fig. 3). The corrected Chl *a* values were then used in the remainder of the study. The concentration of Total Suspended Solids (TSS) was determined using the gravimetric method for non-filterable residue by filtering 100 ml of sample through Whatmann GF/F filters which were dried at 105° C in an oven for at least 2 hours (EPA, 1983). The inorganic component, Inorganic Suspended Solids (ISS), was determined by burning off the organic component in a muffle furnace at 260° C overnight, and re-weighing the burnt filter papers. The difference between TSS and ISS was taken to be the concentration of Organic Suspended Solids (OSS). Secchi Disk depth (SD), a proxy for water clarity, was estimated using a matt white disk of diameter 15cm using the mean of the depths at which the disk disappeared when lowered into the water and reappeared when brought to the surface, on the sunny side of the boat. Absorption by CDOM (a_{CDOM}) between 250nm and 750nm was measured on the GF/F filtrate using a Shimadzu UV-2501 spectrophotometer. The absorbance spectra were converted to absorption using the following equation, after subtracting the absorbance spectra of water (Milli-Q) (Green & Blough, 1994):

$$a(\lambda) = \frac{2.303A(\lambda)}{I} \quad (m^{-1}) \qquad (1)$$

where $a(\lambda)$ is the absorption coefficient, $A(\lambda)$ is the absorbance, and I is the pathlength (= 0.01 m). A null-point correction was performed at 750 nm and the curves fitted to the following negative exponential function using least-squares case-wise nonlinear estimation (Bricaud et al., 1981):

$$a_y(\lambda) = a_y(\lambda_0)e^{-S(\lambda-\lambda_0)} \quad (m^{-1}) \qquad (2)$$

where $a_y(\lambda_0)$ is the reference absorption at wavelength λ_0, and S is the slope of the curve.

Aerosol Optical Thickness (AOT) at five wavelengths in the visible and near-infrared spectrum (λ = 440, 500, 675, 870, 900 nm) was measured using a handheld Microtops II Sun Photometer V 5.5 (Solarlight Co.). Measurements were made within 30 minutes of MERIS overpasses using the lowest value of four separate scans as the true value. Wind speed and wave height was also measured concurrent to water sample collection. The standard error of the mean of limnological and environmental parameters was determined according to:

Table 2
Independent variables used in empirical algorithms for estimating water quality parameters. Numbers are radiometric wavelengths in nanometres. Algorithms for MERIS used bands nearest to wavelengths given here.

Independent variables	Chl *a*	TSS, ISS, OSS	SD	a_{CDOM}
	560	560	560	412
	700	700	700	442
	Peak~700	Peak~700	Peak~700	(664/559)
	(700/670)	(700/670)	(700/670)	(677/480)
	RLH[1]	RLH	RLH	(559-619)/619[8]
	700/(560+670)[2]	700/(560+670)	700/(560+670)	*Gitelson*[9]
	(560-520)/(560+520)[3]	(560-520)/(560+520)	(560-520)/(560+520)	-
	740((1/670)-(1/710))[4]	-	(520/700)[6]	-
	FLH[5]	-	(490/620)[7]	-

[1] Reflectance Line Height: 700-670-((750-670)×(700-670)/(750-670)) (Schalles et al., 1998)
[2] (Koponen et al., 2007)
[3] (Gitelson et al., 1993)
[4] (Zimba & Gitelson, 2006)
[5] Fluorescence Line Height: 685-670-((730-670)×(685-670)/(730-670)) (Gower et al., 1999)
[6] (Koponen et al., 2002)
[7] (Härmä et al., 2001)
[8] (Kallio et al., 2001)
[9] (453-(700/670)-520)/(453+(700/670)+520) (Gitelson et al., 1993)

$$SE_{\bar{X}} = \frac{s}{\sqrt{n}} = \sqrt{\frac{\sum_{i=1}^{n}(X_i - \bar{X})^2}{n-1}} \times \frac{1}{\sqrt{n}} \quad (3)$$

where s is sample standard deviation, n is sample size, X_i is ith value of X (the parameter) and $\bar{X}$ is the mean. The normality of the data distributions was tested using the Shapiro-Wilks test.

Radiometric measurements were made simultaneous to water sample collection at sample points ZEV 2 and ZEV 3 using a Hyperspectral Tethered Surface Radiometer Buoy (HyperTSRB S/N 018 Satlantic Inc.). The TSRB measures upwelling radiance at depth 0.66 m, $L_u(0.66)$, and downwelling irradiance just above the surface, $E_d(0+)$, in the range 400 to 800 nm at a 3.3 nm resolution with a spectral accuracy of 0.3 nm. The spectra were recorded on a laptop computer using SatView V.2.8 (Satlantic Inc.). The median value for the sampling period (about 3 minutes) was used to obtain a single spectrum for $L_u(0.66)$ and $E_d(0+)$, which was then re-sampled to a 1nm spectral resolution. The in-water radiance/irradiance reflectance at 0.66 m, which has no value for remote sensing although it is useful for analysing the bio-optical variability, was calculated as:

$$R(0.66) = \frac{L_u(0.66)}{E_d(0+)} \quad (4)$$

The normalised water-leaving surface reflectance, ρ_w, was calculated using the upward vertical attenuation coefficient for upward radiance, K_u, according to:

$$\rho_w = \pi \times \frac{L_u(z) \times e^{K_u z}}{E_d(0+)} \times \frac{\eta^2}{\tau} \quad (5)$$

where z is depth in meters and $\frac{\eta^2}{\tau}$ ($=\frac{0.98}{1.33}$) is the constant for the air-water interface correction according to Snell's law.

As the value for K_u was not measured it had to be estimated using the following formulation for optically deep, case 2 water (Albert & Mobley, 2003):

$$K_u(\lambda) = (a(\lambda) + b_b(\lambda)) \times \left(1 + \left(\frac{b_b(\lambda)}{a(\lambda) + b_b(\lambda)}\right)\right)^{3.5421} \times \left(1 + \left(\frac{-0.2786}{\cos\theta_s}\right)\right) \quad (m^{-1}) \quad (6)$$

where $a(\lambda)$ is the total absorption coefficient, $b_b(\lambda)$ is the total backscattering coefficient, and θ_s is the subsurface solar zenith angle.

Although there are problems with using this approximation in turbid waters such as Zeekoevlei, it is likely to be suitable as a first order estimate. The values for $a(\lambda)$ and $b_b(\lambda)$ which were used in (6) where estimated from bio-optical simulations based on a model similar to that used in Stramski et al. (2001) with the following equations:

$$a(\lambda) = a_w(\lambda) + Ca^*_\phi(\lambda) + a_{CDOM}(\lambda) + Na^*_d(\lambda) + Na^*_m(\lambda) \quad (m^{-1}) \quad (7.1)$$

$$b_b(\lambda) = b_{bw}(\lambda) + Cb^*_{b\phi}(\lambda) + Nb^*_{bd}(\lambda) + Nb^*_{bm}(\lambda) \quad (m^{-1}) \quad (7.2)$$

where a^* and b^* are the specific absorption/backscattering coefficients respectively, subscripts w, ϕ, CDOM, d and m stand for water, phytoplankton, CDOM, detritus and minerals, C is concentration and N is the number of particles.

Table 3
Pearson linear correlation coefficients, r, for limnological and environmental parameters. All correlations were significant at p<0.05. Italics indicate parameters which failed the Shapiro-Wilk test for normality.

	Chl a	TSS	ISS	OSS	SD	a_{CDOM}	Wave height	Wind speed
Chl a	1.00							
TSS	0.76	1.00						
ISS	0.59	0.91	1.00					
OSS	0.79	0.93	0.68	1.00				
SD	*-0.79*	*-0.76*	*-0.69*	*-0.70*	1.00			
a_{CDOM}	0.59	0.61	0.50	0.61	*-0.60*	1.00		
Wave height	*0.52*	*0.78*	*0.77*	*0.68*	*-0.57*	*0.61*	1.00	
Wind speed	*0.47*	*0.72*	*0.72*	*0.61*	*-0.51*	*0.71*	*0.75*	1.00

The input data used in Equations 7.1 and 7.2 are shown in Table 1. Importantly the simulations are first order approximations used for deriving ρ_w in the absence of K_u measurements. In order to simulate the co-dominance of cyanophyta and chlorophyta in Zeekoevlei, two marine phytoplankton were weighted equally in their

biomass contribution, as given by Chl *a*. The number of particles for detritus and minerals was determined by their contribution to absorption by particulate matter at 440 nm, $a_p(440)$, as in Stramski et al. (2001). The contribution of detritus was about 17%, and that of minerals about 7%, when using the average *in situ* measurements of Chl *a* (=153.3 mg.m^{-3}) and a_{CDOM} at 440nm (=2.78 m^{-1}) in the model. This gave $N = 6.25\times10^{16}$ for detritus and $N = 2.16\times10^{16}$ for minerals. It was decided to keep the number of particles constant for all simulations to avoid additional sources of error. This is likely to be acceptable as a first-order approximation.

The two main sources of error to ρ_w calculated using (5) are from instrument self-shading and K_u estimates calculated using (6). A simple test was used to evaluate the error introduced to ρ_w from estimating K_u: the value of K_u was varied in percentage over the spectrum while observing the change to ρ_w. A 10% change in the value of K_u gave an average change to ρ_w of 25% in the positive direction, and 20% in the negative direction, in the range 400 to 700 nm. Thus, in this simulation, a change in K_u leads to a change in ρ_w usually at least twice as large as that to K_u. For the sake of simplicity, K_u estimations were assumed to be within 10% of their actual value, which meant an average error of 25% in the positive direction, and 20% in the negative direction. The instrument self-shading error causes $L_u(0.66)$ to be underestimated; and may result in less accurate algorithm performance as the error is wavelength dependent. The total error from self-shading, $\varepsilon(\lambda)$, was calculated according to (Leathers et al., 2001):

$$\varepsilon(\lambda) = \frac{\varepsilon_{sun} + \varepsilon_{sky} f}{1 + f} \quad (8)$$

where ε_{sun} is the error from direct sunlight, ε_{sky} is the error from diffuse skylight and f is the ratio of skylight to direct sunlight.

The values for the errors from direct and diffuse light were calculated using Table 1 in Leathers et al. (2001) using appropriate values for *a(λ)*, the solar zenith angle, and the ratio of $a(\lambda)$ to $b(\lambda)$, which was estimated using the bio-optical model (described above). Values of f were from clear sky summer conditions for the Cape west coast of South Africa (Walters et al., 1985). $L_u(0.66)$ acquired during clear sky conditions were corrected according to (Leathers et al., 2001):

$$L_u^{true}(\lambda) = \frac{L_u^{measured}(\lambda)}{1 - \varepsilon(\lambda)} \qquad (Wm^{-2}sr^{-1}nm^{-1}) \quad (9)$$

where $L_u^{true}(\lambda)$ is the true (corrected) radiance spectrum, and $L_u^{measured}(\lambda)$ is the measured radiance spectrum.

The total error associated with ρ_w was then calculated using the root mean square of the errors from estimating K_u and instrument self-shading.

3.2 Atmospheric correction algorithms

MERIS FR geo-located and calibrated Top-of-Atmosphere (TOA) Radiance (Level 1P) and FR geophysical ocean, land and atmosphere product (Level 2P) was pre-ordered from ESA for April 2008 using the Earthnet OnLine Interactive (Eoli-sa) client V. 6.0.1. The data were processed in the VISAT BEAM (Version 4.2) software toolbox (Brockmann Consult). The Smile Correction Processor (V.1.1.2) plug-in was used to correct for the 'smile effect' and the Radiance-To-Reflectance Processor (V1.3.100) converted the L 1 data to normalised TOA apparent reflectance, ρ_{TOA}, according to the following equation:

$$\rho_{TOA}(\lambda) = \frac{\pi L_{TOA}(\lambda)}{E_0(\lambda)\cos\theta_s} \quad (10)$$

where L_{TOA} is the TOA radiance, E_0 is solar spectral irradiance, that includes earth-sun distance correction, and θ_s is the solar zenith angle.

Water pixels were identified by low reflectance values in the near-infrared bands and extracted from a rectangular area drawn around the lake. The ICOL processor plugin for BEAM may be used to correct L 1 water pixels for the adjacency effect (Santer & Zagolski, 2008). However, the unusually high radiances from Zeekoevlei's turbid water meant that the land mask was overlaid in the L 1 product. This meant that despite efforts, the ICOL processor was not able to be implemented. Thus there is an unaccounted for adjacency effect in the results, although its impact may be less significant because of the relatively large signal from the very turbid water. Atmospheric correction to obtain the water-leaving reflectance from pixels corresponding to the sample points in Fig. 1 was carried out using both image-based techniques, and the 6S Radiative Transfer Code (RTC) (Vermote et al., 1997). The image-based Dark Object Subtraction (DOS) technique eliminates the need for *in situ* measurements of atmospheric properties by using the darkest pixel in the scene as an estimate of the atmospheric path radiance, $L_{\lambda path}$, in all bands, assuming that the atmosphere is homogenous across the entire scene (Chavez, 1996). The dark pixels were taken from shadows in the mountainous region north-east of Cape Town approximately 100 km away from the study site.

At-satellite TOA radiances were corrected to surface reflectances, $\rho(\lambda)$, according to (Moran et al., 1992):

$$\rho(\lambda) = \frac{\pi\left(L_{TOA}(\lambda) - L_{\text{path}}(\lambda)\right)}{T_{\lambda}\uparrow\,(kE_0(\lambda)\times\cos\,\theta_s \times T_{\lambda}\downarrow + E_{down})} \qquad (11)$$

where $T_\lambda\downarrow$ and $T_\lambda\uparrow$ are the downward and upward atmospheric transmittances, respectively, k is the sun-earth distance coefficient that is dependent on the day of the year, and E_{down} is the downwelling spectral irradiance.

The DOS model assumes $T_\lambda\downarrow$ and $T_\lambda\uparrow$ = 1 and ignores the effects of downwelling spectral irradiance (E_{down} = 0). The value for $L_{\lambda\text{path}}$ is extracted from the darkest object in the scene. For comparison the improved cosine or 'COST' method was also used, which estimates $T_\lambda\downarrow$ by the cosine of the solar zenith angle, $cos\theta_s$, and $T_\lambda\uparrow$ by the cosine of the viewing zenith angle, $cos\theta_v$. The values for $E_0(\lambda)$, θ_s, and θ_v taken from the MERIS product. The 6S RTC Version 1.1 (available at http://modis-sr.ltdri.org/6S_code/index.html) was run using a mid-latitude summer atmospheric model and an urban aerosol model. The target was defined as lake water assuming there were no directional effects and a Lambertian surface. The AOT at 550 nm used for the code was estimated by interpolating sun photometer measurements at 500 and 675 nm. Geometrical conditions including month, day, solar zenith and azimuthal angles, and viewing zenith and azimuthal angles, were taken from the MERIS product.

3.3 Water quality parameter algorithms

3.3.1 MERIS NN algorithms

The two MERIS IRTM-NN algorithms were tested for estimating atmospheric properties and water constituent concentrations for Zeekoevlei. The standard Level 2 Case 2 water algorithm uses the atmospherically corrected normalised surface reflectance in 8 bands and the solar zenith, viewing zenith and azimuth difference angles as input to give the concentration of phytoplankton pigments (Chl *a*) in the range 0.003 to 50 mg.m^{-3}, the concentration of TSS in the range 0.03 to 50 g.m^{-3}, and the absorption by *gelbstoff* (CDOM) at 440 nm in the range 0.002 to 2 m^{-1}. The procedure uses a feed forward error-backpropagation multiple nonlinear regression neural network technique which is parameterised using water leaving radiance reflectances generated by Monte Carlo radiative transfer simulations using data collected in North European, Mediterranean and North Atlantic coastal waters (Schiller & Doerffer, 1999, Schiller & Doerffer, 2005). Atmospheric correction is carried out using a coupled hydrological-atmospheric model specifically designed for 'bright-pixel' case 2 waters (Moore et al., 1999). There are several studies which show that the standard product gives good results in European lakes and coastal case 2 waters (Cipollini et al., 2001, Schiller & Doerffer, 2005, Reinart & Kutser, 2006). However, the algorithm is unlikely to perform well in Zeekoevlei's extremely turbid hypertrophic water due to the narrow training range and the suite of IOPs used in the in-water simulations which may differ from those in Zeekoevlei.

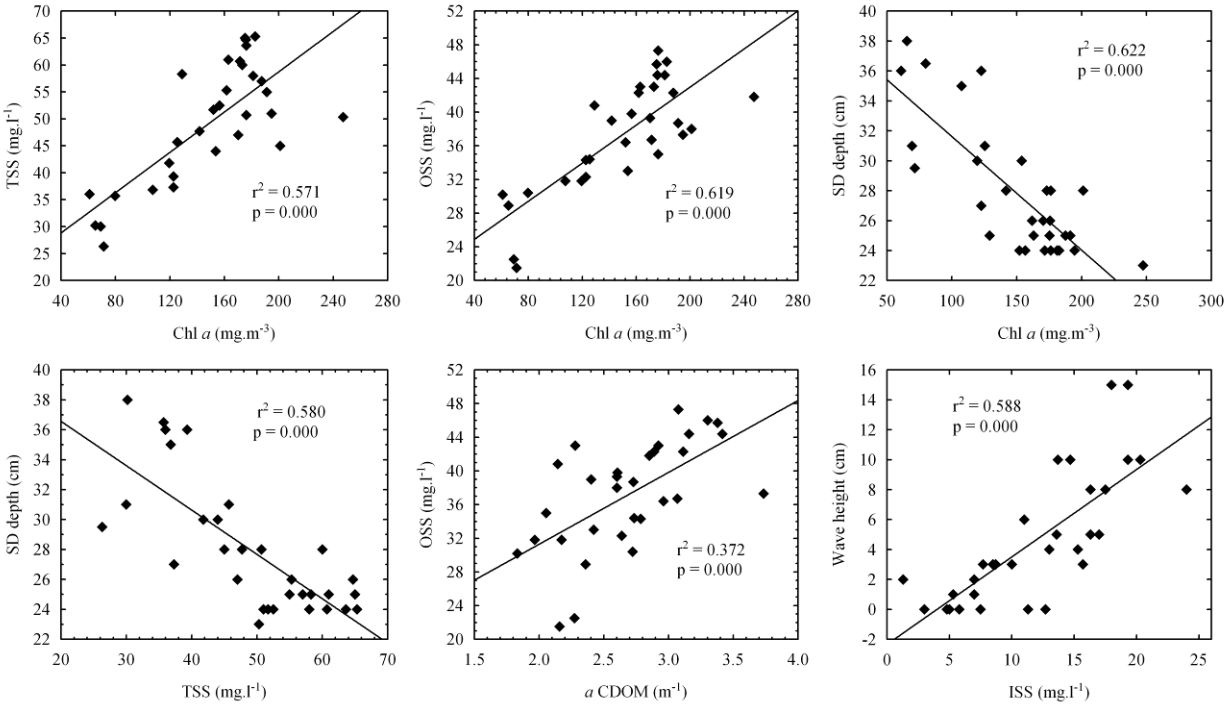

Fig. 2. Scatterplots showing the best-fit regression lines and correlation coefficients between selected parameters. N = 31 for all plots.

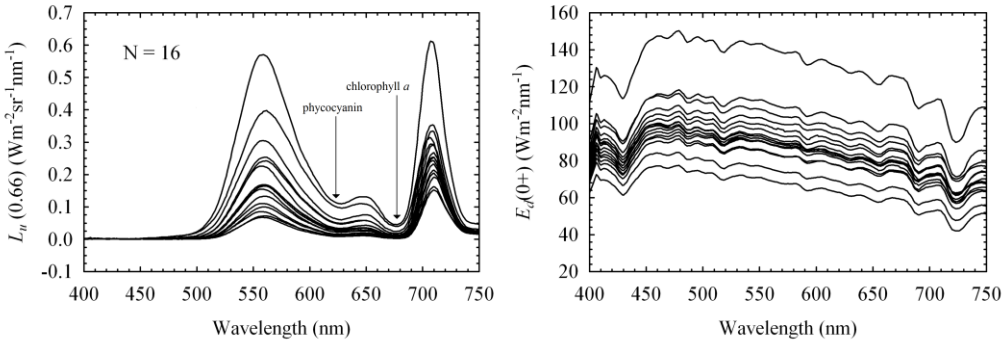

Fig. 3. Sixteen simultaneously collected spectra of upwelling radiance at 0.66 m (left) and downwelling irradiance just above the surface (right) collected from the four sample points between April 1st and 24th 2008. The absorption bands of phytoplankton pigments phycocyanin and Chl *a* are shown.

The Eutrophic Lakes Processor, designed specifically for eutrophic lakes, is likely to produce improved results for Zeekoevlei. The algorithm computes total particulate scattering and absorption by Chl a and *gelbstoff* at 443 nm, as well as Chl *a* and TSS concentrations, the attenuation coefficient for downwelling irradiance at wavelength with maximum transparency (K_{dmin}), and the optical depth from which 90% of the reflected light comes (z_{90}), from the water-leaving reflectance in 8 bands. The water-leaving reflectances from MERIS are produced by an atmospheric correction which uses a forward radiative transfer model which incorporates the bio-optical model (Doerffer & Schiller, 2008a). Therefore, the atmospheric correction is not independent of the water constituent retrieval model. The algorithm is trained using more than 60 000 spectra obtained from bio-optical simulations with the Hydrolight Radiative Transfer Code based on data collected from Finnish and Spanish eutrophic lakes, to derive Chl *a* concentrations in the range 0 to 120 mg.m^{-3}, TSS in the range 0.42 to 50.9 g.m^{-3} and absorption by *gelbstoff* at 440 nm in the range 0.1 to 3 m^{-1} (Doerffer & Schiller, 2008b). The concentrations ranges and IOPs used in these simulations are likely to be more suited to the hypertrophic water in Zeekoevlei.

3.3.2 Empirical algorithms

Empirical algorithms for estimating water quality parameters were formulated using linear and non-linear regression analysis. Algorithms were derived for the radiance/irradiance reflectance at 0.66 m, $R(0.66)$, and for MERIS TOA radiances and reflectances and Bottom-Of-Atmosphere (BOA) atmospherically corrected water-leaving reflectances. Certain empirical algorithms may be suitable for estimating parameters such as Chl *a* from the TOA MERIS signal, hence the use of TOA data and the comparison with algorithms using BOA data types (e.g. Giardino et al., 2005). The single band, band ratio, and band arithmetic variables in Table 2 were utilised as independent variables in the regressions, while the water quality parameters were utilised as the dependent variables. The algorithms in Table 2 were selected on the basis of an investigation of recent studies using empirical procedures in inland waters.Pearson Product moment linear regression analysis was formulated according to the model:

$$y = a + bx \tag{12}$$

where y is the dependent water quality parameter, x is the independent variable (from Table 2) and a and b are regression coefficients.

Case-wise non-linear least squares regression was applied according to the model:

$$y = ax^b \tag{13}$$

The r^2 coefficient of determination gives an indication of the significance of the correlation at the 95% confidence interval (p-value of significance = 0.05). The normality of the data distributions was tested using the Shapiro-Wilk test. The water quality parameters were also log transformed in regressions using the radiometric data, as it is reasonable to assume a non-linear relationship between reflectance and some of the parameters. The F-value, the ratio of explained to unexplained variance, was used to further establish the significance of the correlation at the 95% confidence level. A large F-value indicates that the independent variable, x, may be used to reliably estimate the parameter, y. F-values were calculated according to:

$$F = \frac{s_{\hat{y}}^{\,2}}{s_e^{\,2}} = \frac{\sum_{i=1}^{N}(\hat{Y}_i - \bar{Y}_i)^2}{k} \Bigg/ \frac{\sum_{i=1}^{N}(\hat{Y}_i - Y_i)^2}{N-k-1} \tag{14}$$

where N is the number of observations, $\hat{Y}$ is the predicted value of the water quality parameter, $\bar{Y}$ is the mean of observed water quality parameter, Y is the

observed value the water quality parameter and k is the number of predictors.

The standard error of the residuals, also called the Root of the Mean Square of the Error (RMSE), gave an estimate of the error associated with the estimations according to:

$$s_e(RMSE) = \sqrt{\frac{\sum_{i=1}^{N}(\hat{Y}_i - Y_i)^2}{N-k-1}} \quad (15)$$

Maps were made for each water quality parameter using the best performing empirical algorithms for MERIS. The maps were plotted as pseudo-colour checkerboard plots where each cell in the plot represents a single MERIS pixel and a colour bar indicates the unique value of each pixel. Statistics calculated for the maps included the number of pixels, the area, and the mean, median, minimum and maximum, standard deviation, standard error of the mean and the observed error of the parameters. The standard error of the mean for remotely sensed estimates was calculated using the formula below:

$$SE_{\bar{\hat{Y}}} = s_e \sqrt{\frac{1}{n} + \frac{(X_k - \bar{X})^2}{\sum_{i=1}^{N}(X_i - \bar{X})^2}} \quad (16)$$

where s_e is the standard error of residuals (equation 15), n is number of observations, X_k is the mean value of the independent variable x for all estimations, $\bar{X}$ is the mean of independent variable x for observed values, and X_i is the observed value of independent variable x.

The observed error, the difference between the remotely sensed and *in situ* means, gives the improved accuracy to the mean spatial estimate delivered by using MERIS (Kallio et al., 2003):

$$E = \bar{X}_{insitu} - \bar{X}_{remotelysensed} \quad (17)$$

where $\bar{X}_{insitu}$ is the mean of *in situ* and $\bar{X}_{remotelysensed}$ the mean of remotely sensed parameter estimates.

4. Results

4.1 Limnological conditions

The mean Chl *a* concentration during the sampling period was 148.6 ± 8.1 mg.m^{-3} (N = 31) with a maximum of 247.4 mg.m^{-3} and a minimum of 61.0 mg.m^{-3}. The water colour was bright green with occasional surface accumulations of buoyant cyanobacteria on calm days, especially near the shore. The mean TSS concentration was 49.1 ± 2.0 g.m^{-3} and the mean organic component was 76.9% (N = 31). The total contribution of phytoplankton to OSS was estimated to be between 28 and 35% using a simple conversion factor of 1 mg.m^{-3} Chl *a* ≈ 0.07 - 0.09 g.m^{-3} dry weight derived from similar eutrophic lakes in the Netherlands (Dekker, 1993). The remainder of the organic matter probably originates from detrital material mixed into the water column from the organically rich sediment accumulations on the lake floor (Harding, 1992). Thus, the contribution of phytoplankton, detritus and minerals to TSS was about 25%, 52% and 23% respectively. Water transparency was very low with a mean SD depth of only 27.9 ± 0.8 cm. This meant that the water was optically deep and that bottom effects could be ignored. Absorption by CDOM at 440 nm had a mean value of 2.69 ± 0.08 m^{-1}, while the value of S in equation (2) varied between 0.0169 and 0.0212 with a mean of 0.0188 ± 0.0002 (N = 31), which is typical of other inland waters (Kirk, 1994). A significant degree of covariance was observed between Chl *a*, TSS and OSS (Table 3, Fig. 2). As expected, SD depth is significantly inversely correlated with Chl *a*, suspended solids and a_{CDOM}, as these all decrease water clarity. The weak positive correlation between a_{CDOM} and Chl *a*, TSS and

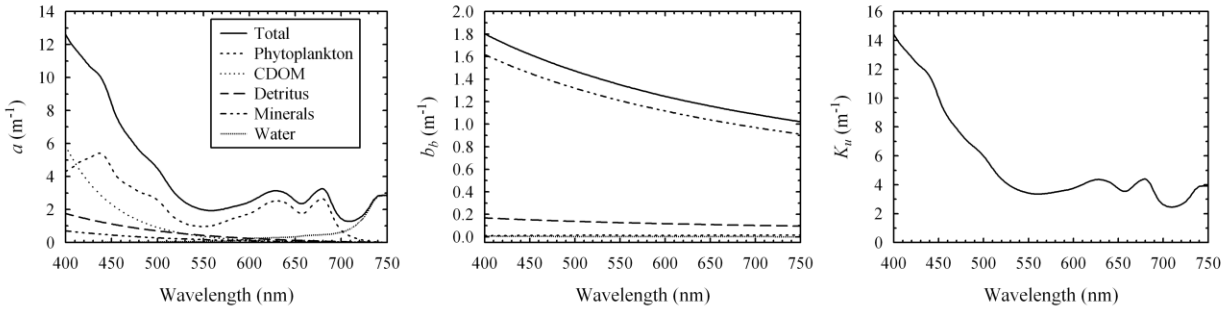

Fig. 4. Components of the total absorption, $a(\lambda)$, (left) and total backscattering, $b_b(\lambda)$, (centre) coefficients used to calculate K_u (right). The values used in the above simulation are as follows: Chl *a* = 153.3 mg.m^{-3}; a_{CDOM}(440 nm) = 2.78 m^{-1}; detritus $N = 6.25\times10^{16}$; minerals $N = 2.16\times10^{16}$.

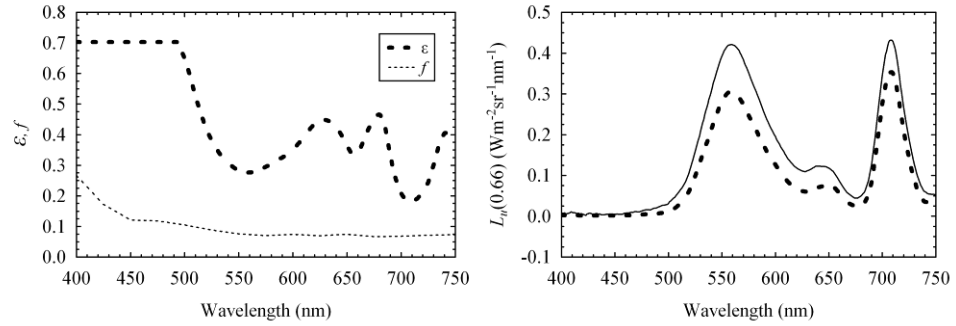

Fig. 5. The total self shading error, ε, and the ratio of skylight to direct sunlight, *f*, (left) and a corresponding measured (dotted line) and corrected (solid line) $L_u(0.66)$ spectrum (right) from sample point 1 measured on the 23rd April 2008.

OSS may be from the generation of humic matter by decomposing plant matter in hypertrophic conditions, as suggested by Kirk (1994). Wave height and wind speed are significantly correlated with suspended solids, especially the inorganic component (although these are non-normally distributed), indicating that bottom sediments are mixed into the surface layers by wind and waves, as described in Harding (1997).

The variability in water conditions across the lake is apparent from comparisons of the mean measurements made at the sample points. The southern basin had higher average Chl *a* concentrations (ZEV3 = 160.5 mg.m^{-3}, N = 10) compared to Home Bay (= 134.0 mg.m^{-3}, N = 6) and the northern basin (= 134.0 mg.m^{-3}, N = 10). The explanation for this increased production may be the underground seepage of nutrients from the adjacent sewage works, which is the lake's major source of nutrients (Southern Waters Ecological Research and Consulting, 2000). The northern basin has the highest mean wave heights (= 6.5 cm, N = 10) and TSS concentrations (= 50.6 g.ℓ$^{-1}$, N = 10) with the highest mean inorganic content. This is most likely a result of mixing of bottom sediment into the water column by the predominant southerly wind. In contrast, the more sheltered Home Bay had the lowest mean wave heights (= 1.8 cm, N = 6) and TSS concentrations (= 45.8 g.ℓ$^{-1}$, N = 6). The calmer conditions in Home Bay promote surface accumulations of buoyant cyanobacteria which results in an increase in mean organic matter contribution (= 78.1%, N = 6) and a decrease in mean SD depths (water clarity) (= 26.7 cm, N = 6). The greater mixing in the northern basin prevents cyanobacteria collecting at the surface and results in lower contributions of organic matter to TSS (= 73.4%, N = 10) and increased SD depths (= 28.8 cm, N = 10). Therefore, it appears that wind and wave action, and the input of nutrients from the sewage works, are the main drivers of spatial variability in Zeekoevlei, although the differences between the sample points is relatively small.

4.2 Apparent optical properties and bio-optical model

4.2.1. L_u*(0.66) and* E_d*(0+)*

Fig. 3 shows 16 concurrent upwelling radiance, $L_u(0.66)$, and downwelling irradiance, $E_d(0+)$, spectra obtained during April 2008. The $L_u(0.66)$ spectra show two distinct peaks at about 560 and 710 nm as a result of the processes of scattering and absorption from the optically active components. The unusually flat signal from 400 to 470 nm appears to be caused by strong absorption from high concentrations of detritus and mineral particles (*tripton*) which make up about 75% of TSS. *Tripton*, which absorbs most strongly in the blue (Babin & Stramski, 2002), has been found to be the main absorbing component in other similar eutrophic lakes (Simis et al., 2005). High concentrations of Chl *a* (430 nm) and CDOM also contribute to the high absorption in the blue. The absorption maximums of phytoplankton pigments Chl *a* (~680 nm) and

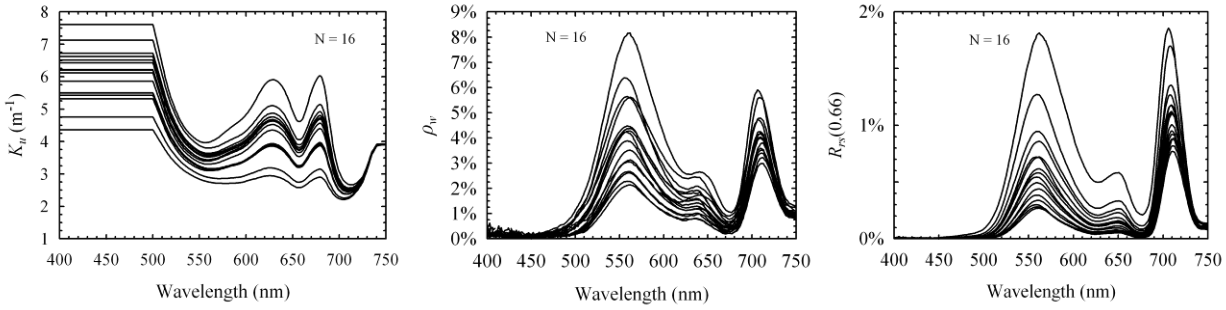

Fig. 6. Spectral K_u plots (left) used to calculate the normalised water leaving reflectance, ρ_w, (centre) for spectra collected from the four sample points between April 1st and 24th 2008. The reflectance at 0.66 m, $R(0.66)$ is also shown(right) .

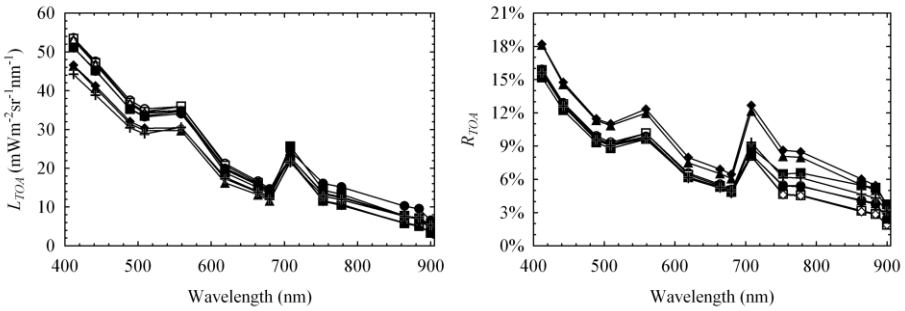

Fig. 7. MERIS TOA smile corrected radiance (left) and TOA reflectance (right) for nine pixels acquired on the 1st, 7th, 20th and 23rd April, corresponding to simultaneously acquired *in situ* measurements. The oxygen absorption band at 761 nm has been excluded.

phycocyanin (~620 nm) are characteristic of the cyanobacteria-dominated phytoplankton assemblage (e.g. Schalles et al., 1998, Simis et al., 2007). The upwelling radiance is relatively spectrally invariant suggesting that the IOPs were mostly constant, at least in constituent-relative composition, during the sampling period. The $E_d(0+)$ spectra display the characteristic absorption bands of ozone, oxygen and water vapour, and differ in magnitude as a result of variable sky conditions and differing times of measurement (between 9 and 12 am).

4.2.2. Calculation of $\varepsilon(\lambda)$, K_u *and* ρ_w

The bio-optical model (section 3.1.2) gave absorption values comparable to the upper range of those measured in similar eutrophic waters (~4 m^{-1} at 665 nm) (Fig 4.) (Dall'Olmo & Gitelson, 2005, Simis et al., 2005). However, in the blue (<500 nm) the $a(\lambda)$ values appear very large, probably a result of the inability of the model to account for the offset to absorption by scattering from suspended matter. The large $a(\lambda)$ in the blue produced erratic values when calculating $L_u^{true}(\lambda)$ and ρ_w using $\varepsilon(\lambda)$ and K_u. Therefore the values for $\varepsilon(\lambda)$ and K_u at wavelengths less than 500 nm were held constant at their value at 500 nm (Fig. 5, Fig. 6). While the values for $\varepsilon(\lambda)$ and K_u are somewhat synthetic, they are likely to be acceptable since $L_u(0.66)$ in this region is very close to zero. Fig. 5 shows a $L_u(0.66)$ spectra

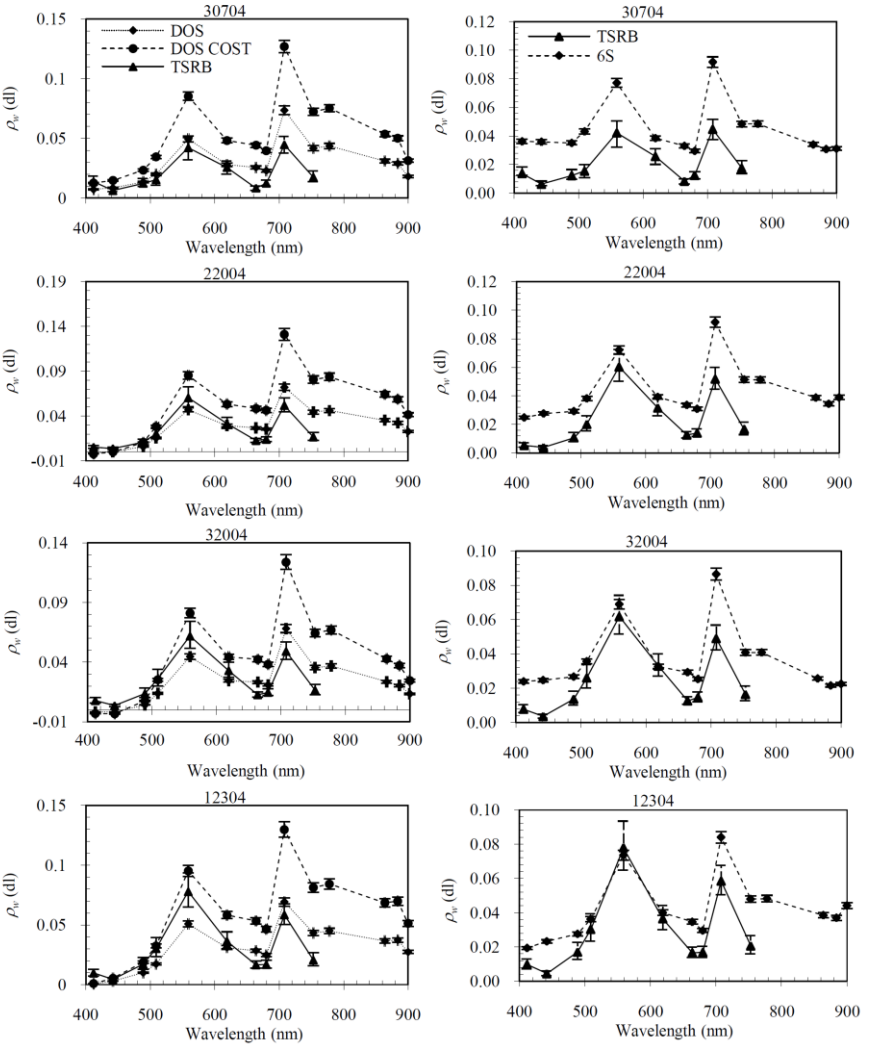

Fig. 8. Comparison between image-based Dark Object Subtraction (DOS) and Cosine (COST) (left hand column), and 6S (right hand column) atmospheric corrections. Corresponding radiometric spectra measured *in situ* (TSRB) (corrected for self-shading) give an idea of algorithm performance. The error bars show systematic error from MERIS (5%) and that from estimating K_u. The number above the graphs indicates the sample point followed by the day and month, for example, 30704 is sample point 3 on the 7th of April 2008.

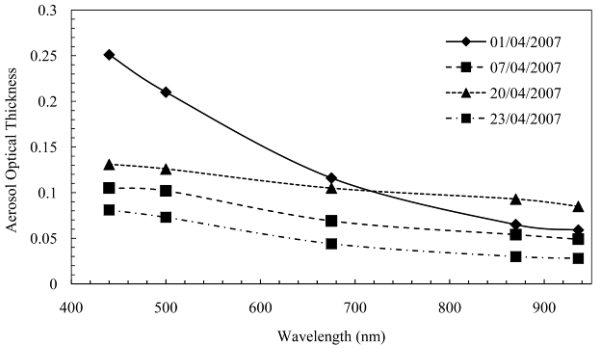

Fig. 9. Aerosol optical thickness measured near simultaneous to the acquisition of MERIS on four days in April 2008.

measured in clear sky conditions at sample point 1 on April 23rd 2008 corrected for self-shading. As expected, the corrected spectrum shows increased magnitude relative to the uncorrected one. Table 1 in Leathers et al. (2001) had to be extrapolated to obtain the self-shading error, which was lessened by diffuse scattering since $b(\lambda) >> a(\lambda)$. The mean self-shading error over the wavelengths 500 to 750 nm was approximately 36%. The calculated ρ_w spectra are comparable in shape and magnitude to those measured in other similar eutrophic waters (Fig. 6) (Dekker, 1993, see Schalles et al., 1998, Simis et al., 2007). The $R(0.66)$ spectra calculated using equation (9) also have very similar spectral shapes. The differing magnitudes of the spectra indicate variable backscattering from changes in the concentrations of suspended particulates whose optical properties appear to be relatively spectrally invariant.

4.3 Atmospheric correction algorithms

14 MERIS scenes were acquired over Zeekoevlei during April 2008. Four of these were cloud free and had corresponding *in situ* measurements. These match-up data were used for evaluating atmospheric corrections and for deriving and testing water quality parameter algorithms (section 4.4). Fig. 7 shows the TOA smile corrected radiance and reflectance spectra for nine pixels corresponding to simultaneously acquired *in situ* measurements in Zeekoevlei. The spectral shapes are similar to those measured radiometrically with distinctive peaks visible in the 559 and 708 nm bands, and the characteristic absorption maxima of phytoplankton pigments Chl *a* (664 and 680 nm) and phycocyanin (620 nm). The large signal in the blue (<500 nm) is the result of atmospheric scattering (Gordon, 1978). Four of these pixels which had corresponding *in situ* radiometric water-leaving reflectance measurements have been atmospherically corrected and are presented in Fig. 8. Overall, the agreement between the atmospheric corrections and the *in situ* measurements is likely to be acceptable for a first order application in complex waters. However, the image based DOS and COST corrections (left hand column in Fig. 8) have some negative values in the 412 and 442 nm bands signifying an overestimation of the atmospheric path radiance by the dark object in these bands. The reflectance in the infrared (>700 nm) is also overestimated which is most likely a caused by adjacency effects (Santer & Schmechtig, 2000). Between the two techniques the simpler DOS model appears to give better agreement with *in situ* measurements. The image-based corrections also appear to introduce a spectral bias in some of the bands which will cause algorithms to operate less accurately. Therefore, image-based procedures are used infrequently in water remote sensing because of these inconsistencies and are suboptimal with regard to automated processing. The 6S RTC corrections (right hand column Fig. 8) appear to introduce less spectral bias. However, the model as applied here also seems to under-correct in the near-infrared and blue regions of the spectrum, again which is most likely the result of the adjacency effect (especially visible in the bands near 900 nm). Fig. 9 shows the AOT measurements acquired within less than 10 minutes of the MERIS overpass on the four days. The figure provides some information on the variability of atmospheric conditions occurring between these days and reveals that atmospheric conditions vary within a range of optical thickness of about 1.4 at 500 nm. The slope of the AOT (the Angstrom coefficient, α) is greatest for April 1st but does not vary greatly on the other days. Therefore, as the atmospheric variability is quite small, it is reasonable to assume that the atmosphere is not a great source of error in the derivation of empirical algorithms from MERIS (section 4.4.3).

4.4 Water quality parameter algorithms

4.4.1 MERIS NN algorithms

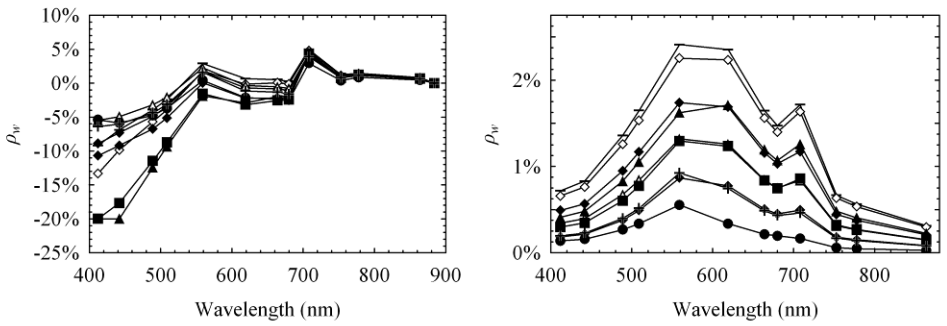

Fig. 10. Normalised water-leaving reflectance spectra generated from the standard Level 2 product (left) and Eutrophic Lakes processor (right) for nine pixels corresponding to *in situ* sample points.

Pixels for Zeekoevlei from the MERIS Level 2 product were invariably flagged as 'invalid turbid case 2 sediment-dominated water'. Flags were also raised for water constituent retrieval and occasionally for aerosol retrieval. This means that the values derived by the standard Level 2 product are suspect, as confirmed by Fig. 10 which shows the spectra for the nine pixels. The standard product correctly identifies Zeekoevlei's water type but the negative reflectance values in the blue indicate that the atmospheric correction failed. The most plausible explanation for the failure is a breakdown of the assumption of negligible water-leaving radiance in the near infra-red, as a result of the very high sediment concentrations in Zeekoevlei, and possibly the sediment type (Aiken & Moore, 2000). The chance that the failure was caused by the presence of anomalous atmospheric conditions seems highly unlikely since AOT measurements made *in situ* where within normal ranges (see Table 4, Fig. 9). Corresponding spectra from the Eutrophic Lakes processor, shown on the right hand side in Fig. 10, had no negative values although the spectral shapes are somewhat uncharacteristic, especially at 619 nm where the values are inflected, and at 509 nm and other bands in the blue, where the values are enlarged relative to *in situ* measurements (see Fig. 6). Not surprisingly, there are large discrepancies between water constituent concentrations and atmospheric properties estimated by the NN algorithms and those measured *in situ* (Table 4). Chl *a* and TSS concentrations are severely underestimated by the standard L 2 product, a_{CDOM} is overestimated, albeit only slightly, and AOT at 443 nm has negative values. The Eutrophic Lakes processor gives improved Chl *a* and TSS estimates, especially for April 1st, however the remainder of the estimates were once again well below observed values. The AOT values at 550 nm are comparable to *in situ* measurements at 500 nm suggesting that the errors in water constituent retrieval may be due to differences in the concentration ranges and IOPs used to train the bio-optical model, rather than due to failures in atmospheric correction. This explanation is also evidenced by the uncharacteristic spectral shapes observed in Fig. 10. Discrepancies between the IOPs used in the bio-optical model and those of Zeekoevlei also cause errors in the atmospheric correction, as the atmospheric correction is based on the same training data set used to derive the IOPs (Doerffer & Schiller, 2008a). The large errors in estimation observed in Table 4 emphasize the regional specific nature of the default NN algorithms and the need to re-parameterise them with local IOP measurements.

4.4.2. Empirical algorithms for R(0.66)

The correlation between radiance/irradiance reflectance,

Table 4
Comparison between *in situ* measurements and results from the MERIS C2R and Eutrophic Lakes NN algorithms.

	In Situ					Level 2				Eutrophic Lakes Processor			
Sample No.	Chl *a*	TSS	a_{CDOM}	AOT 440	AOT 500	Chl *a*	TSS	a_{CDOM}	AOT 443	Chl *a*	TSS	a_{CDOM}	AOT 550
10104	69.2	30.0	2.27	0.251	0.210	7.9	8.2	3.24	-0.006	19.7	29.6	1.28	0.268
20104	61.0	36.0	1.83	0.251	0.210	27.1	19.6	4.17	-0.006	20.9	40.8	1.16	0.243
30104	71.3	26.3	2.16	0.251	0.210	7.9	8.2	3.34	-0.006	21.0	39.6	1.23	0.241
40104	107.5	36.8	1.97	0.251	0.210	8.2	9.5	3.13	-0.006	19.2	21.7	1.20	0.265
20704	119.5	41.8	2.17	0.104	0.102	9.5	3.8	4.04	-0.006	10.9	3.7	0.53	0.074
30704	247.4	50.3	2.85	0.104	0.102	10.6	4.8	3.91	-0.006	20.2	18.5	1.04	0.213
22004	171.5	60.7	3.07	0.13	0.125	10.6	4.8	3.91	-0.006	18.9	12.1	0.94	0.254
32004	194.6	51.0	3.73	0.13	0.125	10.2	5.1	3.79	-0.006	20.6	29.7	1.51	0.250
12304	122.6	37.3	2.78	0.081	0.073	7.9	7.6	3.24	-0.006	18.1	10.1	0.68	0.092

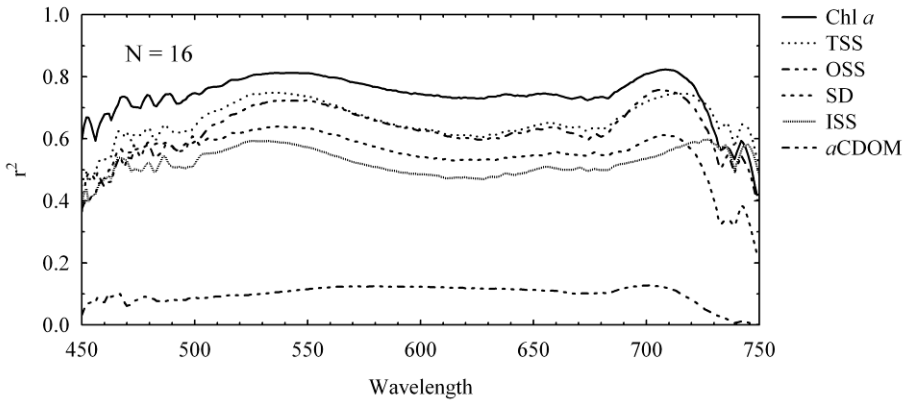

Fig. 11. The correlation between $R(0.66)$ and the water quality parameters.

$R(0.66)$, and the water quality parameters was tested at a 1nm resolution in order to determine the optical influence of the constituents (Fig. 11). The correlations for Chl a, TSS, OSS, and ISS are in a negative direction since reflectance is inversely related to these constituents; and in a positive direction for SD as larger values indicate less turbid water. The very similar shapes of the correlation curves are most likely caused by the significant covariance between the parameters. The correlation with Chl *a* and suspended solids is quite significant across almost the entire spectrum, reaching the highest values (~0.8) at the reflectance peaks near 540 and 710 nm. Significant correlations were also observed between Chl *a* and the magnitude and position of the reflectance peak near 700 nm normalised at 640 nm, in agreement with findings in other eutrophic waters (Gitelson, 1992, Schalles et al., 1998). This reflectance peak is likely to be caused by the strong absorption of phytoplankton around 675 nm, strong and sharply increasing absorption by water in the near-infrared, and strong backscattering from phytoplankton and suspended matter > 700 nm, causing a sharp reflectance peak (Gitelson, 1992, Yacobi et al., 1995). The ISS correlation curve reaches its highest value near 730 nm most likely because inorganic minerals contribute strongly to scattering in the near-infrared, and water is the dominant and invariant cause of strong absorption. The correlation with a_{CDOM} is not significant as the signal from CDOM is significant only in the blue region of the spectrum which was not plotted due to noise. Importantly, Fig. 11 shows that for Zeekoevlei, the reflectance peaks near 540 and 710 nm can best be used to estimate the concentrations of water constituents. From a causal perspective it appears that scattering from gross particulate load is the dominant IOP in these very turbid conditions, given the lack of absorption by water constituents at these wavelengths. Therefore it is not surprising that algorithms in Table 2 incorporating bands near 710 and 550 nm give the best performance for Chl *a* and suspended solids estimations (Table 5).

The Reflectance Line Height (RLH) algorithm gave a r^2 value of 0.856 for Chl *a*, which is consistent with those derived by Schalles et al. (1998) (=0.83) and Yacobi et al. (1995) (=0.98) in similar eutrophic waters. The algorithm based on the three band conceptual model proposed by Zimba and Gitelson (2006) for hypertrophic water performed less well (r^2 = 0.657), although the performance could perhaps be improved by tuning the model (Dall'Olmo & Gitelson, 2005). The

Table 5
Correlation coefficients (r^2) for empirical algorithms using $R(0.66)$. N = 16. Non-significant correlations are in italics.

Algorithm	Chl *a*	LnChl *a*	TSS	LnTSS	ISS	LnISS	OSS	LnOSS	SD	LnSD
RLH	0.771	0.856	0.709	0.763	0.470	0.640	0.774	0.809	0.669	0.661
700	0.762	0.854	0.713	0.770	0.481	0.661	0.766	0.802	0.666	0.656
Peak~700	0.729	0.833	0.751	0.802	0.525	0.676	0.782	0.816	0.672	0.659
(700/670)	0.627	0.600	0.661	0.654	*0.358*	*0.409*	0.849	0.839	0.478	0.491
(560-520)/(560+520)	0.516	0.566	0.874	0.870	0.620	0.650	0.897	0.895	0.566	0.566
700/(560+670)	0.671	0.680	0.773	0.776	0.477	0.542	0.897	0.898	0.601	0.610
560	0.737	0.852	0.713	0.780	0.505	0.715	0.733	0.775	0.681	0.666
FLH	0.667	0.767	-	-	-	-	-	-	-	-
740((1/670)-(1/710))	0.657	0.578	-	-	-	-	-	-	-	-
(520/700)	-	-	-	-	-	-	-	-	0.684	0.679
(490/620)	-	-	-	-	-	-	-	-	0.531	0.500

Table 6
r^2 correlation coefficients of empirical algorithms. Non-significant correlations ($p<0.05$) are in italics. N = 9.

Algorithms	Data type				
	L_{TOA}	R_{TOA}	ρ_{wDOS}	ρ_{wCOST}	ρ_{w6S}
Chl *a*					
(708/664)	0.925	0.925	*0.093*	*0.093*	0.784
RLH	0.910	0.887	0.918	0.812	0.865
708	*0.252*	*0.252*	0.702	0.626	0.800
753((1/664)-(1/708))	0.808	0.782	0.712	0.712	0.772
TSS					
(708/664)	0.691	0.691	*0.013*	*0.013*	0.634
RLH	0.542	0.501	0.718	0.712	0.741
708	*0.091*	*0.091*	0.655	0.625	0.810
708/(559+664)	0.763	0.760	0.753	0.753	0.792
ISS					
(559-509)/(559+509)	*0.437*	*0.437*	*0.044*	*0.044*	*0.114*
708/(559+664)	*0.378*	*0.372*	*0.433*	*0.433*	0.483
708	*0.014*	*0.014*	*0.283*	*0.274*	0.455
OSS					
(708/664)	0.763	0.763	*0.012*	*0.012*	0.566
RLH	0.666	0.626	0.745	0.724	0.647
708	*0.147*	*0.147*	0.678	0.641	0.697
708/(559+664)	0.721	0.725	0.638	0.638	0.639
SD					
(708/664)	0.801	0.801	*0.025*	*0.025*	0.685
RLH	0.624	0.600	0.805	0.822	0.756
708	*0.056*	*0.056*	0.690	0.693	0.697
(509/708)	0.687	0.687	*0.052*	*0.052*	0.556
a_{CDOM}					
Gitelson*	*0.398*	0.751	*0.144*	*0.134*	0.630
412	0.610	0.610	0.466	*0.442*	*0.249*
442	0.618	0.618	*0.140*	*0.129*	*0.289*
(559-619)/619	*0.372*	*0.372*	*0.033*	*0.033*	*0.204*
*(442 - (708/664) - 509)/(442 + (708/664) + 509)					

700/670 band ratio algorithm did not perform better than the single band algorithms in this instance. The reflectance difference ratio algorithm 560-520/560+520 for TSS gave an $r^2 = 0.874$, higher than that derived by Gitelson et al. (1993) ($r^2 = 0.86$) in European inland waters. The difference ratio algorithm also gave the strong correlations for OSS and ISS ($r^2 = 0.897$ and 0.620, respectively). The 700/560+670 band ratio algorithm gave equally strong results for OSS ($r^2 = 0.897$). The best performance for SD was given by the band ratio algorithm 520/700 ($r^2 = 0.684$).

The outcome that different empirical algorithms appear to perform equally well for a number of parameters is the result of the highly covariant data set and the existence of non-unique signals from parameters such as phytoplankton and TSS. Therefore the empirical algorithms cannot be expected to give similar results in other studies where the statistical properties of the data set are substantially different from those used here. Importantly, the high level of covariance means that the empirical algorithms are limited in their ability to account for – and separate – signals from the different water constituents, and therefore show changes in gross particulate matter, rather than from individual independent parameters. Importantly, the empirical algorithms cannot be expected to achieve the same performance when being used in conditions dissimilar to those of Zeekoevlei.

4.4.3 Empirical algorithms for MERIS

Table 6 shows the results of the regression analysis using the algorithms in Table 2 using MERIS match-ups. The five MERIS data types used in the regressions were TOA smile corrected radiance (L_{TOA}), TOA reflectance (R_{TOA}), DOS (ρ_{wDOS}) and COST (ρ_{wCOST}) corrected normalised water-leaving reflectances, and 6S corrected normalised water-leaving reflectance (ρ_{w6S}).

The algorithm performance, indicated by the correlation coefficient, is strongly affected by the data type. In general, single band algorithms perform better with atmospherically corrected data while band ratio algorithms work better with TOA data. This is because ratio algorithms normalise the atmospheric effects so long as the bands are near to each other spectrally (e.g. 709/664). It is also evident that the image-based atmospheric corrections, which estimate the path radiance by a dark object, cause erratic algorithm performance due to the introduction of spectral bias. In contrast, ρ_{w6S} is associated with robust algorithm performance emphasising the desirability of a physically sound radiative transfer correction over simpler image-based techniques. It is also clear from Table 6 that most of the algorithms appear to perform equally well for most of the parameters. This is the result of the strong covariance between many of the parameters in the small data set (N=9).

Table 7
Empirical algorithms derived from TOA MERIS reflectance (R_{TOA}) used for creating maps.

Empirical Algorithms	r^2	t	P	F	RMSE	N
Chl *a* = 5.931 (708/664) $^{5.934}$	0.964	-	0.0000	563.3	9.8%	9
TSS = –84.428 + 218.329 (708/(559+664))	0.760	4.7	0.0022	22.2	14.1%	9
OSS = –37.411 + 41.934 (708/664)	0.763	4.7	0.0021	22.5	10.9%	9
SD = 79.469 – 30.596 (708/664)	0.801	-5.3	0.0011	28.2	8.0%	9
a_{CDOM} = – 25.137 – 31.806 (*Gitelson**)	0.751	-4.6	0.0025	21.1	13%	9
ISS = 30.600 – 479.079 (559-509)/(559+509)	0.437	-2.3	0.0524	5.4	56.9%	9
*(442 - (708/664) - 509)/(442 + (708/664) + 509)						

In terms of algorithm performance, the 708/664 band ratio algorithm using TOA data gave the highest correlation for Chl *a*. Using nonlinear estimation (Equation 15) with the same data type, the correlation coefficient was improved to 0.965 (Table 7). The strong non-linear relationship between Chl *a* and the 708/664 band ratio observed here is well-documented in other eutrophic waters (Gitelson et al., 1993, Jiao et al., 2006, Menken et al., 2006). The 708/664 algorithm also performed very well for estimating the significantly covariant parameters TSS, OSS and SD. Other algorithms which gave good results for Chl *a* are Zimba and Gitelson's (2006) hypertrophic waters algorithm and the RLH algorithm. These algorithms are more robust than the 708/664 algorithm as they are relatively unaffected the data type. The 708 band algorithms give substantially better correlations with Chl *a* after atmospheric correction, as well as for all the other parameters. The most robust predictor of TSS is the 708/(560+664) algorithm, although the highest correlation was produced by the single band 708 algorithm. The highest correlations for ISS were achieved before atmospheric correction with the (559-509)/(559+509) difference ratio algorithm, and after atmospheric correction with the 708/(560+664) algorithm. Algorithm performance for OSS is very similar to that for Chl *a*, as phytoplankton make up on average about 32% of OSS. All algorithms gave high correlations for SD, expectedly so as the Secchi disk depth is a good proxy for gross particulate load. Besides for ISS, a_{CDOM} was the most difficult to predict of the parameters. Gitelson's band ratio algorithm which accounts for the effects of pigment absorption by including the 708/664 ratio, gave good performance from TOA and BOA data types. The lack of causal explanation for the correlations with the 412 and 442

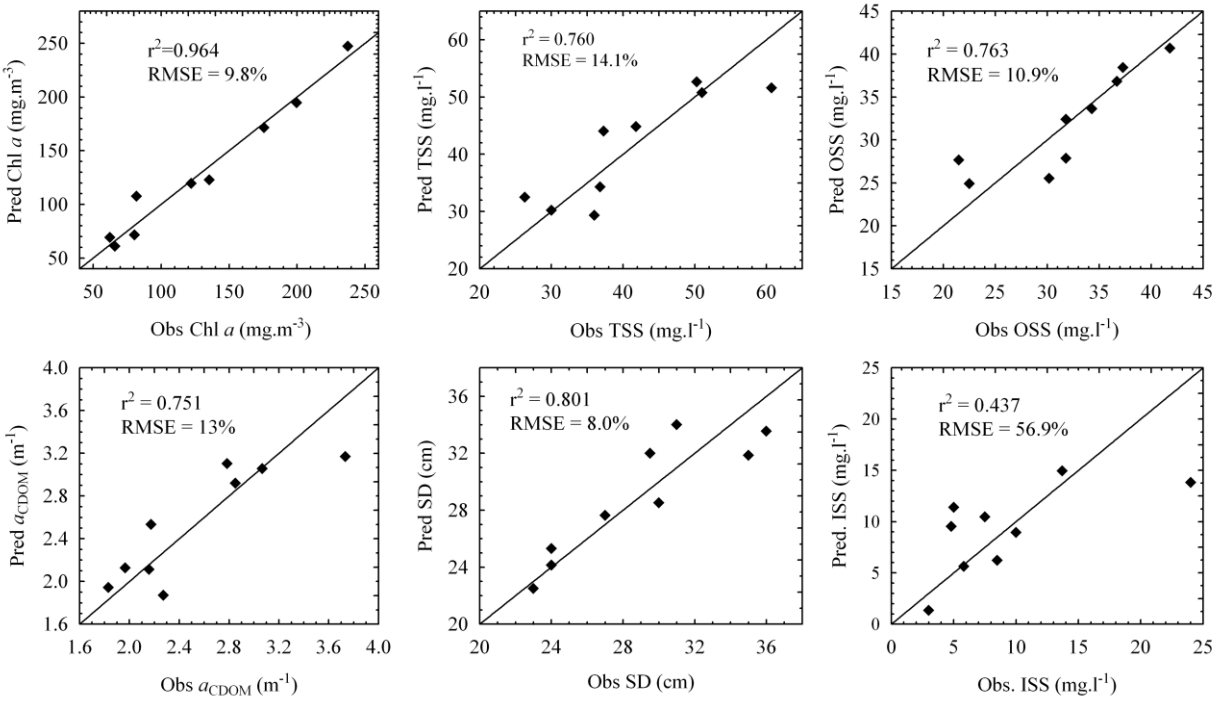

Fig. 12. Observed versus predicted water quality parameters derived from MERI TOA reflectance (R_{TOA}) with empirical algorithms.

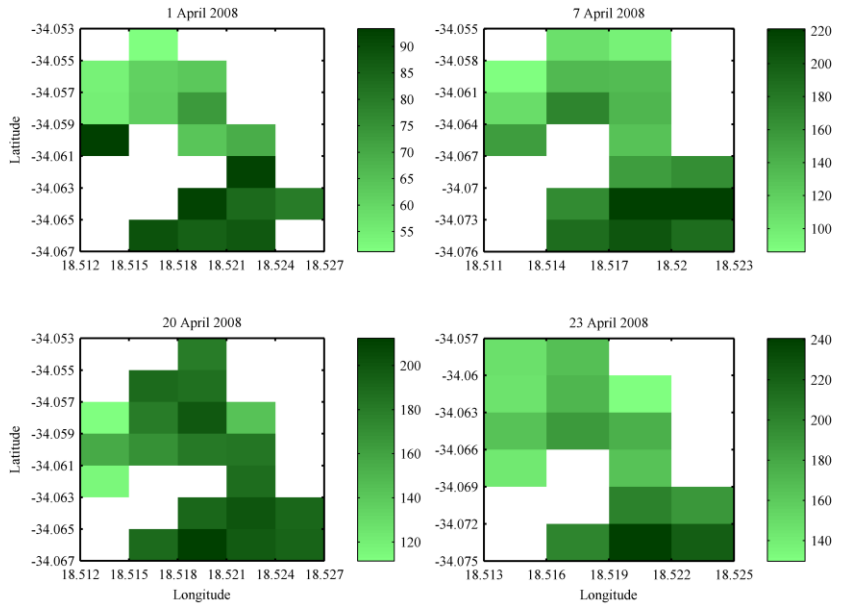

Fig. 13. Checkerboard plots of Chl *a* derived from an empirical algorithm using MERIS TOA reflectance (R_{TOA}) for four days in April 2008. Units are in mg.m^{-3}. Note differences in colour bar scales.

single TOA bands has already been noted above. Overall, for algorithms using TOA reflectance more than 75% of the variation of the parameters (besides ISS) could be explained with a RMSE of less than 15% (Table 7, Fig. 12). The t-statistics and F-values show that the variance is well explained and that the band ratios/combinations can reliably be used to predict the parameters. The considerable degree of covariance between the parameters means that the algorithms effectively show changes in gross particulate loading rather than in individual parameters. The relative stability of the atmospheric conditions between MERIS scenes, shown in Fig. 9, means that the atmosphere is not a significant source of error in the derivation of the algorithms, especially since the algorithms employ band ratios. Importantly, the algorithms are only valid for the in-water and atmospheric conditions from which they are derived.

4.5 Maps

Fig. 13 shows maps of Chl *a* created from four cloud-free MERIS scenes using the empirical algorithm in Table 7. The surface area of the maps range between 110 and 150 ha at the 260×290 m MERIS pixel resolution, which is well below the 256 ha total surface area of the lake. As far as possible the pixels used in mapping are from the central 'core' area of the lake, reducing the chance of including erroneous 'land' pixels. The maps differ in size and shape because the number of pixels varied between 15 and 20, and some duplicated pixels were removed. The longitudes and latitudes on the maps were taken directly from the level 1 MERIS scene and not further geo-corrected. The environmental conditions measured *in situ* corresponding to the maps are shown in Table 8. These are used to explain the spatial variability of the parameters visible on the maps. Fig. 13 shows appreciable variation in the magnitude and the spatial distribution of Chl *a* in Zeekoevlei on the four days. The southern basin appears to have higher sustained Chl *a* concentrations than the northern basin which, as previously explained, is most likely caused its proximity to the WWTW which is the largest source of nutrients to the lake. The prevailing wind and wave conditions seem to be correlated to the Chl *a* variability, especially in the northern basin. The very calm conditions experienced on the morning of April 1st coincided with markedly lower Chl *a* concentrations than on the other days (maximum of 87.2 mg.m^{-3}); while on April 20th the high concentrations observed in the northern basin coincided with a strong southerly breeze. These observations suggest that mixing by wind and wave action has a significant effect on the phytoplankton (or suspended solids) density at the surface. In a shallow lake such as Zeekoevlei, mixing drives primary production through offsetting the effects of light limitation and algal self-shading. Harding (1997) found that for Zeekoevlei, wind speeds greater than or equal to 2 - 3 m.s^{-1} are sufficient for mixing the upper 0.5 m of the water column, and speeds of greater than approximately 6 m.s^{-1} are sufficient for mixing to the mean depth of the lake (1.9 m), provided a fetch of between 750 and 1000 m. Therefore we can assume that on the 20th of April the lake was mixed to the mean depth at least in some regions. On this day, mixing of negatively-buoyant chlorophyta from the subsurface water layers and sediments from the lake floor led to the observation of higher apparent Chl *a* concentrations at the surface (especially in the northern basin). It is also plausible that phytoplankton from the more productive southern basin may have been transported to the northern basin by the strong southerly wind. According to Scott et al. (1969) buoyancy by cyanobacteria is offset in wind speeds exceeding approximately 3.7 m.s^{-1} (= 13.3 km.hr^{-1}).

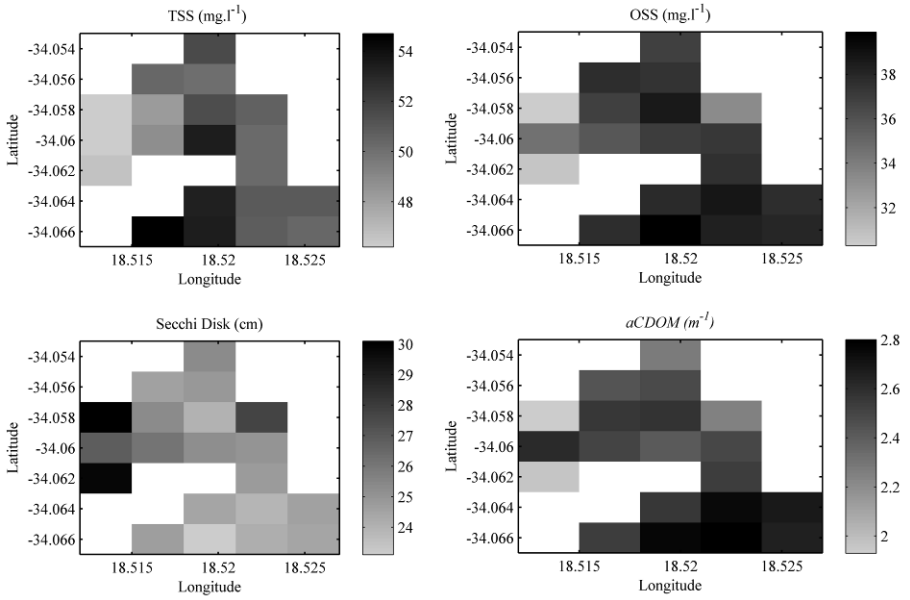

Fig. 14. Checkerboard plots of TSS, OSS, SD and a_{CDOM} for April 20th 2008 derived from MERIS TOA reflectance (R_{TOA}) using empirical algorithms.

measurements is decreased through using remote sensing. The observed error, the difference between mean remotely sensed and *in situ* measurements, is as large as -30%. Therefore, assuming that the true mean for Zeekoevlei is the remotely sensed estimate, estimates of the mean using *in situ* measurements alone in this example may be up to 30% in error, although this error is reduced by increasing the number of sample points.

Fig. 14 shows maps for the remaining parameters from April 20th created using the empirical algorithms in Table 7. Maps were not drawn for ISS because the correlation coefficient was not significant. The maps all display patterns very similar or identical to that of Fig. 13. This is mainly due to the fact that the algorithms for Chl *a*, OSS, SD and a_{CDOM} all make use of the 708/664 band ratio and so vary in proportion with each other. As a consequence, the position and shading of pixels (concentrations distributions) are identical although they have different values. This is one potential drawback associated with empirical algorithms, and it illustrates the limited ability they have to separate signals from different parameters when there is a significant degree of covariance. The TSS map shows a somewhat different pattern, as the algorithm uses a slightly altered band ratio, but also clearly shows higher concentrations in the southern basin and lower concentrations in the northern basin near the mouths of the Lotus Rivers. The divergence, albeit small, between the TSS and Chl *a* maps may be explained by the inorganic contribution to TSS. The observation of higher TSS concentrations coincided

Table 8
Environmental variables measured *in situ* simultaneous to MERIS overpasses

Date	Points Sampled	Sky conditions	Wind speed & direction		Wave height	Water Temp.	Water colour
01/04	1 – 4	Clear.	0 $m.s^{-1}$	-	0 cm	21.5° C	Bright green with surface bloom.
07/04	2 – 3	Partly cloudy.	1.9 $m.s^{-1}$	S	3 cm	19.8° C	Medium green.
20/04	2 – 3	Clear. High cirrus.	5.3 $m.s^{-1}$	SE	9 cm	18.6° C	Dark green.
23/04	Pier	Clear.	1.4 $m.s^{-1}$	SW	0 cm	20.1° C	Bright green with surface bloom.

This explains the absence of surface accumulations on windy days and their appearance in parts of the lake on April 1st and 23rd. However, the appearance of cyanobacteria on the surface during calm conditions did not lead to higher Chl *a* concentrations. This may be caused by a reduction in the overall phytoplankton density at the surface due to the absence of mixing of non-byoyant phytoplankton from the subsurface layers, or as a result of high levels of sunlight which causes chlorophyll photo-oxidation (Nelson, 1993). Therefore, it appears that wind and waves are the dominant factor affecting the spatial variability and magnitudes of Chl *a* concentrations visible on the maps. Statistical analysis of the maps shows how remote sensing can lead to improved estimates of the mean spatial values of Chl *a* in Zeekoevlei. The standard error of the mean for *in situ* samples ranged from 7.8 to 50.8% (calculated using Equation 3). In contrast the standard error of the mean for remote sensing estimates (calculated using Equation 16) was smaller, ranging from 2.3 to 6.9%. Thus the large uncertainties involved with estimating the mean concentration for the lake with only a few *in situ*

with windy conditions supporting the suggestion that wave action mixes negatively-buoyant phytoplankton and sediments composed mainly of organic detritus from the lake floor to the surface. The SD map (dark shading denotes greater water clarity) most visibly reveals the clearer water conditions in the northern basin. Further statistical analysis revealed that the observed error for the mean spatial estimate of TSS may be as large as 20% when using only one sample point. However, the observed errors were not as large for OSS, SD and a_{CDOM} owing to the small range of values for these parameters.

5. Discussion

5.1 Limnological conditions

The limnological conditions during April 2009 were typical of those measured previously in Zeekoevlei (Harding, 1992). The mean concentrations of Chl *a* and TSS were very high (148.6 $mg.m^{-3}$ and 49.1 $g.m^{-3}$), and mean water clarity as measured by Secchi disk was very low (27.9 cm). Absorption by CDOM at 440nm (not previously published for Zeekoevlei) ranged between 1.83 and 3.73 m^{-1} with a mean of 2.69 m^{-1}, typical of other inland waters (N = 31) (e.g. Kirk, 1994). The value of the slope coefficient S ranged between 0.0169 and 0.0212 with a mean of 0.0188 (N = 31). The majority of TSS was detritus (about 52%), with phytoplankton and minerals composing the remaining 25% and 23%, respectively. There was significant covariance between all of the limnological parameters which had implications for algorithm development and performance. The maps produced from MERIS showed the temporal and spatial variability and range of the parameters in a synoptic manner unequalled by conventional monitoring techniques. This provides valuable information for management and enhanced understanding of the spatial and temporal dynamics of cyanobacteria-dominated algal blooms and water quality in Zeekoevlei. There was little overall spatial variability in the parameters, with only somewhat higher production in the southern basin and slightly clearer water in the northern basin near the inlets of the Great and Little Lotus Rivers. The variability in spatial patterns and concentrations observed between the four days was most likely caused by the wind and wave climate. Windy conditions were associated with higher Chl *a* and suspended solids concentrations resulting from transportation and vertical mixing of negatively-buoyant phytoplankton and sediments dominated by organic detritus from the subsurface water layers and lake floor. Therefore, wind and waves appear to be the main driving mechanism behind water quality variability in Zeekoevlei, in agreement with the hypothesis that wind induced mixing has profound effects on the primary production in the lake, which has been shown to be limited by temperature and the attenuation of photosynthetically active irradiance (Harding, 1997). The presence of sustained increased production in the southern basin was attributed to underground nutrient seepage from the adjacent Waste Water Treatment Works. The standard error of mean parameter estimates was reduced through using MERIS.

5.2 Apparent optical properties

In situ measurements of upwelling radiance were strongly dominated by absorption from *tripton* composed of detritus and minerals, phytoplankton pigments and CDOM, and scattering from suspended inorganic matter. There was very little upwelling light in the blue (<500 nm), strong absorption minima at ~620 and ~680 nm characteristic of phycocyanin and Chl *a* pigments, and strong reflectance peaks at ~560 and ~710 nm. The shapes and magnitudes of the water-leaving reflectance spectra were comparable to those measured in other hypertrophic/eutrophic waters with cyanobacteria-dominated phytoplankton assemblages (Dekker, 1993, Dall'Olmo & Gitelson, 2005, Simis et al., 2007). The sharp peak near 710 nm was significantly correlated with Chl *a* and suspended solids (Gitelson, 1992). It appears that scattering by gross particulate load is the dominant causal IOP in these very turbid waters. The relative invariance of the shapes of the spectra indicates that the IOPs were relatively constant for the duration of sampling. Assuming this is true, the differing magnitudes of the spectra are likely to be caused by variable concentrations of phytoplankton and TSS, which, as already discussed, is regulated by the physical wind environment.

5.3 Atmospheric corrections

Zeekoevlei's turbid hypertrophic water and small size presented a challenging case for atmospheric correction. Nevertheless, there was excellent agreement between the spectral shape and magnitude of atmospherically corrected MERIS spectra and those measured *in situ*. This finding confirms that MERIS is useful for detecting accurate water-leaving spectra for eutrophication and cyanobacterial bloom applications in small, hypertrophic water bodies. The image-based corrections introduced a spectral bias and negative values in the blue which the 6S correction avoided. Therefore the physically robust 6S radiative transfer correction is preferable to the image based techniques used here, and could be included in automated processing procedures conditional upon the availability of AOT input data for the code. Such data could be provided through, for example, the Aerosol robotic remote aerosol properties retrieval Network (AERONET). More recently developed atmospheric

correction schemes such as the Self-Contained Atmospheric Parameters Estimation for MERIS data (SCAPE-M) which uses a MODTRAN radiative transfer code based LUT to derive atmospheric properties over land pixels which is then extrapolated over those of adjacent water (Guanter et al., 2009), and techniques employing bands in the short wave infra-red (Shi & Wang, 2009), were not considered in this paper, but may provide significant improvements of atmospheric correction over turbid waters. The adjacency effect, which was not corrected for, was visible as enlarged reflectance values especially in the near-infrared bands. The effect does not seem to greatly reduce the strength of empirical algorithms because of the large signal from the turbid water. In future, alternative correction schemes such as those used in SCAPE-M or others (Brando & Dekker, 2003, Candiani et al., 2007), should be considered alongside the ICOL processor.

5.4 MERIS NN and empirical algorithms

The results of the MERIS L 2 and Eutrophic Lakes Processor NN algorithms demonstrate well the inadequacy of many current semi-analytical algorithms to cope with small hypertrophic turbid water bodies. The products produced poor comparisons with optical and geophysical *in situ* measurements, giving negative reflectances and reflectances with uncharacteristic shapes and magnitudes, and generally grossly underestimating Chl *a*, TSS and a_{CDOM}. The reasons for the failure of the NN algorithm gives insight into the potential drawbacks associated with semi-analytical procedures in hypertrophic waters. Firstly, semi-analytical type algorithms are highly dependent on the accurate retrieval of water-leaving reflectance by atmospheric correction and break down when it fails. As a consequence, so long as atmospheric correction over turbid water remains a challenging task, the usefulness of semi-analytical approaches may be limited in these environments. Since bio-optical models are based on simulations of the water-leaving reflectance, input of incorrect water-leaving reflectances from satellites will inevitably cause water constituent retrieval to fail, especially for optimisation solutions such as Neural Networks which iterate to minimise the difference between observed and predicted water-leaving reflectance spectra. Secondly, the non- applicability of many bio-optical models in terms of IOPs and concentration ranges to hypertrophic conditions limits the usefulness of semi-analytical procedures. This is especially true in instances where the atmospheric correction and bio-optical model are coupled, such as for the Eutrophic Lakes processor. Therefore, current semi-analytical algorithms require more accurate atmospheric correction procedures (see section 5.3 for suggestions) and correct parameterisation of bio-optical models to validate their use in turbid hypertrophic lakes. Unfortunately, re-parameterising the MERIS NN algorithms was outside of the scope of this study owing to the scarcity of inland IOP measurements in southern Africa.

In general, the empirical algorithms derived from both *in situ* and MERIS radiances/reflectances were able to estimate the water quality parameters with a high degree of confidence. In particular, the 700, 700/670, 700/(560+670), and RLH algorithms worked well in the hypertrophic turbid water owing to the high correlation of Ch *a* and TSS with the peaks near 700 and 560 nm. The highest correlation for estimating Chl *a* was achieved with a TOA 708/664 MERIS reflectance ratio algorithm which had a r^2 value of 0.96 and a standard error of only 9.8% (N = 9). This finding again confirms the effectiveness of the 708/664 TOA reflectance ratio and the high potential that MERIS has for monitoring hypertrophic turbid waters (See also Giardino et al., 2005, Gitelson et al., 2009, Moses et al., 2009b, Moses et al., 2009a). Thus it appears that atmospheric correction is not a prerequisite for Chl *a* estimation in hypertrophic lakes when using empirical type procedures and MERIS. The different algorithms were variably sensitive to atmospheric correction: in general single band algorithms improved after atmospheric correction, while algorithms such as RLH and 708/664 were more robust with TOA data. In terms of algorithm performance a radiative transfer atmospheric correction was superior to the image based procedures. It is important to adequately consider the limitations of the empirical procedures used in this study. The empirical algorithms (from MERIS) were derived from a small data set (N = 9) displaying considerable covariance, which meant that many of the algorithms performed, or at least appeared to perform, equally well for a number of parameters (e.g. Chl *a*, TSS and SD). In reality however, the empirical algorithms are probably limited to detecting changes in gross particulate matter composed of material with non-unique signals rather than changes in the individual parameters *per se*. While the empirical algorithms are only applicable for use in this study, it is expected that using the same bands will give equally strong results in other similar turbid hypertrophic waters.

A comparison between the semi-analytical and empirical algorithms shows that while the advantages of semi-analytical type algorithms favour their use in operational water quality monitoring systems, this study demonstrates the considerable potential value for simple TOA algorithms for hypertrophic systems. Whilst remotely-sensed analysis of water quality for sub-hypertrophic inland waters still presents significant

challenges with regard to atmospheric and in-water algorithms, it thus appears the detection of hypertrophy across inland water bodies could be achieved using relatively simple TOA algorithms. In order to improve semi-analytical algorithm performance it is recommended that AERONET sites be established to improve knowledge of atmospheric variability and improve atmospheric corrections, and that IOP measurements specific to eutrophic/hypertrophic southern African inland waters be made. Regional algorithms (empirical and semi-analytical) enabling better estimates of water quality and rapid assessment of the status and trends of environmental threats such as eutrophication and HABs in inland waters would be of immense benefit for southern Africa.

6. Conclusion: inland water quality monitoring with MERIS

The results of the study indicate the feasibility of using MERIS (or future similar medium resolution sensors) for monitoring water quality in hypertrophic inland waters. The specifications of the MERIS sensor, its frequent data acquisition, 300 m pixel resolution, high signal-to-noise ratio, and number and position of spectral bands, make it suited to regular/real-time monitoring applications observing change occurring over short time scales. MERIS's relatively coarse spatial resolution was found to be adequate to derive significant information even for small lakes such as Zeekoevlei. A comparison between correlation coefficients of algorithms using the hyperspectral radiance/irradiance reflectance, and those using MERIS wavebands, reveals that, in this study, there is only a slight advantage in using a hyperspectral resolution sensor over the multispectral MERIS channels. This is due to the position and number of MERIS bands, which allow the application of various empirical and semi-analytical algorithms. In conclusion, MERIS is suitable for monitoring water quality parameters and cyanobacteria-dominated algal blooms in a small hypertrophic lake such as Zeekoevlei, despite the challenges related to its small size and turbid water conditions. The potential of MERIS for detecting specific cyanobacterial pigments such as phycocyanin should be investigated directly in future (e.g. Simis et al., 2005, Kutser et al., 2006). The findings present substantial opportunities for improving monitoring of other inland and coastal waters with similar water quality problems. It is recommended that remote sensing be integrated into inland water quality monitoring programs in southern Africa in order to better determine the regional status and trends of environmental threats from eutrophication and algal blooms.

7. Acknowledgements

Candice Haskins for information on Zeekoevlei. Asieff Khan and the interns at the Zeekoevlei Nature Reserve for assistance with fieldwork. Trevor Probyn and others at Marine and Coastal Management Laboratories in Seapoint for assistance with the laboratory analysis. Andre Du Randt for the TSRB. Annick Bricaud for providing the Chl *a* specific absorption/backscattering spectra. European Space Agency for MERIS data. The University of Cape Town for funding.

8. References

Ahn, Y.H., Bricaud, A., & Morel, A. (1992). Light backscattering efficiency and related properties of some phytoplankters. *Deep-Sea Research, 39*, 1835-1835

Aiken, J., & Moore, G. (2000). Algorithm theoretical basis document: case 2 (S) bright pixel atmospheric correction. *Centre for Coastal & Marine Sciences, PO-TN-MEL-GS-0005*, Plymouth Marine Laboratory

Albert, A., & Mobley, C. (2003). An analytical model for subsurface irradiance and remote sensing reflectance in deep and shallow case-2 waters. *Optics Express, 11*, 2873-2890

Babin, M., & Stramski, D. (2002). Light absorption by aquatic particles in the near-infrared spectral region. *Limnol.Oceanogr, 47*, 911-915

Brando, V.E., & Dekker, A.G. (2003). Satellite hyperspectral remote sensing for estimating estuarine and coastal water quality. *IEEE Transactions on Geoscience and Remote Sensing, 41*, 1378-1387

Bricaud, A., Morel, A., & Prieur, L. (1981). Absorption by dissolved organic matter of the sea (yellow substance) in the UV and visible domains. *Limnol.Oceanogr, 26*, 43-53

Brönmark, C., & Hansson, L.A. (2002). Environmental issues in lakes and ponds: current state and perspectives. *Environmental Conservation, 29*, 290-307

Candiani, G., Giardino, C., & Brando, V.E. (2007). Adjacency effects and bio-optical model regionalisation: MERIS data to assess lake water quality in the subalpine ecoregion. In ESA/ESRIN (Ed.), *Proceedings of the Envisat symposium, 23 - 27 April* Montreaux, Switzerland

Chavez, P.S. (1996). Image-based atmospheric corrections - revisited and improved. *Photogrammetric Engineering & Remote Sensing, 62*, 1025-1036

Chen, Z.Q., Hu, C.M., & Muller-Karger, F. (2007). Monitoring turbidity in Tampa Bay using MODIS. *Remote Sensing of Environment, 109*, 207-220

Ciotti, A.M., & Bricaud, A. (2006). Retrievals of a size parameter for phytoplankton and spectral light absorption by colored detrital matter from water-leaving radiances at SeaWiFS channels in a continental shelf region off Brazil. *Limnology and Oceanography: Methods, 4*, 237-253

Cipollini, P., Corsini, G., Diani, M., & Grasso, R. (2001). Retrieval of sea water optically active parameters from

hyperspectral data by means of generalized radial basis function neural networks. *IEEE Transactions on Geoscience and Remote Sensing, 39*, 1508-1524

Dall'Olmo, G., & Gitelson, A.A. (2005). Effect of bio-optical parameter variability on the remote estimation of chlorophyll-a concentration in turbid productive waters: experimental results. *Applied Optics, 44*, 412-422

de Villiers, S., & Thiart, C. (2007). The nutrient status of South African rivers: concentrations, trends and fluxes from the 1970s to 2005. *South African Journal of Science, 103*, 343-349

Dekker, A. (1993). Detection of optical water quality parameters for eutrophic waters by high resolution remote sensing. *Ph.D., Free University*, Amsterdam

Doerffer, R., & Schiller, H. (2008a). MERIS regional coastal and lake case 2 water project - atmospheric correction Algorithm Theoretical Basis Document (ATBD). *GKSS Research Centre, 1.0*, Geesthacht

Doerffer, R., & Schiller, H. (2008b). MERIS lake water algorithm for BEAM Algorithm Theoretical Basis Document (ATBD). *GKSS Forschungszentrum, 1.0*, Geesthacht

Downing, J.A., Prairie, Y.T., Cole, J.J., Duarte, C.M., Tranvik, L.J., Striegl, R.G., et al. (2006). The global abundance and size distribution of lakes, ponds, and impoundments. *Limnology and Oceanography, 51*, 2388-2397

Downing, J.A., Watson, S.B., & McCauley, E. (2001). Predicting Cyanobacteria dominance in lakes. *Canadian Journal of Fisheries and Aquatic Sciences, 58*, 1905-1908

DWAF. (2003). Trophic status report: trophic status of impoundments. *South African Department of Water Affairs and Forestry, 1*, Pretoria

EPA. (1983). Residue, non filterable method 160.2 (gravimetric, dried at 103-105°C). In US Environmental Protection Agency (Ed.), *Methods for chemical analysis of water and waste* (pp. 160 2.1-160 2.3). Cincinnati, Ohio: Environmental Monitoring and Support Laboratory Office of Research and Development

Falconer, I.R. (2001). Toxic cyanobacterial bloom problems in Australian waters: risks and impacts on human health. *Phycologia, 40*, 228-233

Giardino, C., Candiani, G., & Zilioli, E. (2005). Detecting chlorophyll-a in Lake Guarda using TOA MERIS radiances. *Photogrammetric Engineering & Remote Sensing, 71*, 1045-1051

Giardino, C., Brando, V.E., Dekker, A.G., Strömbeck, N., & Candiani, G. (2007). Assessment of water quality in Lake Garda (Italy) using Hyperion. *Remote Sensing of Environment, 109*, 183-195

Giardino, C., Pepe, M., Brivio, P., Ghezzi, P., & Zilioli, E. (2001). Detecting chlorophyll, Secchi disk depth and surface temperature in a sub-alpine lake using Landsat imagery. *The Science of The Total Environment, 268*, 19-29

Gitelson, A. (1992). The peak near 700 nm on radiance spectra of algae and water: relationships of its magnitude and position with chlorophyll concentration. *International Journal of Remote Sensing, 13*, 3367-3373

Gitelson, A., Garbuzov, G., Szilagyi, F., Mittenzwey, K., Karnieli, A., & Kaiser, A. (1993). Quantitative remote sensing methods for real-time monitoring of inland waters quality. *International Journal of Remote Sensing, 14*, 1269-1295

Gitelson, A.A., Gurlin, D., Moses, W.J., & Barrow, T. (2009). A bio-optical algorithm for the remote estimation of the chlorophyll-a concentration in case 2 waters. *Environmental Research Letters, 4*, 045003

Gordon, H.R. (1978). Removal of atmospheric effects from satellite imagery of the oceans. *Applied Optics, 17*, 1631-1636

Gower, J.F.R., Doerffer, R., & Borstad, G.A. (1999). Interpretation of the 685nm peak in water-leaving radiance spectra in terms of fluorescence, absorption and scattering, and its observation by MERIS. *International Journal of Remote Sensing, 20*, 1771-1786

Green, S.A., & Blough, N.V. (1994). Optical absorption and fluorescence properties of chromophoric dissolved organic matter in natural waters. *Limnology and Oceanography, 39*, 1903-1916

Grobicki, A., Males, R., Martinez, I., Matika, S., & Archibald, S. (2001). Integrated catchment management in an urban context: the Great and Little Lotus Rivers, Cape Town. *Water Research Commission, 864/1/01*, Pretoria

Guanter, L., Ruiz-Verdú, A., Odermatt, D., Giardino, C., Simis, S., Estellés, V., et al. (2009). Atmospheric correction of ENVISAT/MERIS data over inland waters: Validation for European lakes. *Remote Sensing of Environment, doi:10.1016/j.rse.2009.10.004*

Harding, W.R. (1997). Phytoplankton primary production in a shallow, well-mixed, hypertrophic South African lake. *Hydrobiologia, 344*, 87-102

Harding, W.R. (1992). Zeekoevlei - water chemistry and phytoplankton periodicity. *Water Sa, 18*, 237-246

Harding, W.R., Rowe, N., WEssels, J.C., Beattie, K.A., & Codd, G.A. (1995). Suspected toxicosis of a dog attributed to the cyanobacterial (blue-green algal) hepatotoxin nodularin in South Africa. *Journal of the South African Veterinary Association, 66*, 256-259

Härmä, P., Vepsalainen, J., Hannonen, T., Pyhalahti, T., Kamari, J., Kallio, K., et al. (2001). Detection of water quality using simulated satellite data and semi-empirical algorithms in Finland. *The Science of the total environment, 268*, 107-121

Haskins, C. (2006). Zeekoevlei draw down: investigation of water quality in the Big and Little Lotus Rivers and in Zeekoevlei during the 2004 and 2005 annual draw down. *City of Cape Town Scientific Services, Internal Report*, Cape Town

Holm-Hansen, O., Lorenzen, C.J., Holmes, R.W., & Strickland, J.D.H. (1965). Fluorometric Determination of Chlorophyll. *Journal du Conseil, 30*, 3

Jiao, H.B., Zha, Y., Gao, J., Li, Y.M., Wei, Y.C., & Huang, J.Z. (2006). Estimation of chlorophyll a concentration in Lake

Tai, China using in situ hyperspectral data. *International Journal of Remote Sensing, 27*, 4267-4276

Johnk, K.D., Huisman, J., Sharples, J., Sommeijer, B., Visser, P.M., & Stroom, J.M. (2008). Summer heatwaves promote blooms of harmful cyanobacteria. *Global Change Biology, 14*, 495-512

Kallio, K., Koponen, S., & Pulliainen, J. (2003). Feasibility of airborne imaging spectrometry for lake monitoring—a case study of spatial chlorophyll a distribution in two meso-eutrophic lakes. *International Journal of Remote Sensing, 24*, 3771-3790

Kallio, K., Kutser, T., Hannonen, T., Koponen, S., Pulliainen, J., Vepsalainen, J., et al. (2001). Retrieval of water quality from airborne imaging spectrometry of various lake types in different seasons. *The Science of the total environment, 268*, 59-77

Kirk, J.T.O. (1994). *Light and photosynthesis in aquatic ecosystems.* Bristol: J.W. Arrowsmith

Koponen, S., Pulliainen, J., Kallio, K., & Hallikainen, M. (2002). Lake water quality classification with airborne hyperspectral spectrometer and simulated MERIS data. *Remote Sensing of Environment, 79*, 51-59

Koponen, S., Attila, J., Pulliainen, J., Kallio, K., Pyhälahti, T., Lindfors, A., et al. (2007). A case study of airborne and satellite remote sensing of a spring bloom event in the Gulf of Finland. *Continental Shelf Research, 27*, 228-244

Kutser, T. (2004). Quantitative detection of chlorophyll in cyanobacterial blooms by satellite remote sensing. *Limnology and Oceanography, 49*, 2179-2189

Kutser, T., Metsamaa, L., Strömbeck, N., & Vahtmäe, E. (2006). Monitoring cyanobacterial blooms by satellite remote sensing. *Estuarine, Coastal and Shelf Science, 67*, 303-312

Kutser, T., Pierson, D.C., Kallio, K.Y., Reinart, A., & Sobek, S. (2005). Mapping lake CDOM by satellite remote sensing. *Remote Sensing of Environment, 94*, 535-540

Leathers, R., Downes, T.V., & Mobley, C. (2001). Self-shading correction for upwelling sea-surface radiance measurements made with buoyed instruments. *Optics Express, 8*, 561-570

Lee, Z.P., Carder, K.L., & Arnone, R.A. (2002). Deriving inherent optical properties from water color: a multiband quasi-analytical algorithm for optically deep waters. *Appl.Opt, 41*, 5755-5772

Matthews, M.W. (2009). Remote sensing of water quality parameters in Zeekoevlei, a hypertrophic, cyanobacteria-dominated lake, Cape Town, South Africa. *M.Sc., University of Cape Town*, Cape Town

Menken, K.D., Brezonik, P.L., & Bauer, M.E. (2006). Influence of chlorophyll and Colored Dissolved Organic Matter (CDOM) on lake reflectance spectra: implications for measuring lake properties by remote sensing. *Lake and Reservoir Management, 22*, 179-190

Mooij, W.M., Janse, J.H., De Senerpont Domis, L.N., Hülsmann, S., & Ibelings, B.W. (2007). Predicting the effect of climate change on temperate shallow lakes with the ecosystem model PCLake. *Hydrobiologia, 584*, 443-454

Moore, G.F., Aiken, J., & Lavender, S.J. (1999). The atmospheric correction of water colour and the quantitative retrieval of suspended particulate matter in Case II waters: application to MERIS. *International Journal of Remote Sensing, 20*, 1713-1733

Moran, M.S., Jackson, R.D., Slater, P.N., & Teillet, P.M. (1992). Evaluation of simplified procedures for retrieval of land surface reflectance factors from satellite sensor output. *Remote Sensing of Environment, 41*, 169-184

Moses, W., Gitelson, A., Berdnikov, S., & Povazhnyy, V. (2009a). Satellite estimation of chlorophyll-a concentration using the red and NIR bands of MERIS—the Azov Sea case study. *IEEE Geosci.Remote Sens.Lett, 6*, 845

Moses, W.J., Gitelson, A.A., Berdnikov, S., & Povazhnyy, V. (2009b). Estimation of chlorophyll-a concentration in case II waters using MODIS and MERIS data—successes and challenges. *Environmental Research Letters, 4*, 045005

Nelson, J.R. (1993). Rates and possible mechanism of light-dependent degradation of pigments in detritus derived from phytoplankton. *Journal of Marine Research, 51*, 155-179

Oberholster, P.J., Botha, A.M., & Cloete, T.E. (2005). An overview of toxic freshwater cyanobacteria in South Africa with special reference to risk, impact and detection by molecular marker tools. *Biokemistri, 17*, 57-71

Odermatt, D., Heege, T., Nieke, J., Kneubühler, M., & Itten, K. (2008). Water quality monitoring for Lake Constance with a physically based algorithm for MERIS data. *Sensors, 8*, 4582-4599

Onderka, M., & Pekarova, P. (2008). Retrieval of suspended particulate matter concentrations in the Danube River from Landsat ETM data. *Science of the Total Environment, 397*, 238-243

Pápista, É., Ács, É., & Böddi, B. (2002). Chlorophyll-a determination with ethanol–a critical test. *Hydrobiologia, 485*, 191-198

Pegau, S., Zaneveld, J.R.V., Mitchell, B.G., Mueller, J.L., Kahru, M., Wieland, J., et al. (2003). Inherent optical properties: instruments, characterizations, field measurements and data analysis protocols. In J.L. Mueller, G.S. Fargion, & C.R. McClain (Eds.), *Ocean Optics Protocols For Satellite Ocean Color Sensor Validation, Revision 4, Volume IV* (pp. 39-65). Goddard Space Flight Space Center, Greenbelt, Maryland: National Aeronautical and Space Administration

Reinart, A., & Kutser, T. (2006). Comparison of different satellite sensors in detecting cyanobacterial bloom events in the Baltic Sea. *Remote Sensing of Environment, 102*, 74-85

Robarts, R.D., & Zohary, T. (1984). Microcystis aeruginosa and underwater light attenuation in a hypertrophic lake (Hartbeespoort Dam, South Africa). *Journal of Ecology, 72*, 1001-1017

Santer, R., & Zagolski, F. (2008). Improve Contrast between Ocean and Land (ICOL): Algorithm Theoretical Basis

Document (ATBD): The MERIS Level-1C. *Université du Littoral Côte d'Opale, ADRINORD*, France

Santer, R., & Schmechtig, C. (2000). Adjacency effects on water surfaces: primary scattering approximation and sensitivity study. *Applied Optics, 39*, 361-375

Sartory, D.P., & Grobbelaar, J.U. (1984). Extraction of chlorophyll a from freshwater phytoplankton for spectrophotometric analysis. *Hydrobiologia, 114*, 177-187

Schalles, J.F., Gitelson, A.A., Yacobi, Y.Z., & Kroenke, A.E. (1998). Estimation of chlorophyll a from time series measurements of high spectral resolution reflectance in an eutrophic lake. *Journal of Phycology, 34*, 383-390

Schiller, H., & Doerffer, R. (2005). Improved determination of coastal water constituent concentrations from MERIS data. *IEEE Transactions on Geoscience and Remote Sensing, 43*, 1585-1591

Schiller, H., & Doerffer, R. (1999). Neural network for emulation of an inverse model operational derivation of Case II water properties from MERIS data. *International Journal of Remote Sensing, 20*, 1735-1746

Scott, J.T., Myer, G.E., Stewart, R., & Walther, E.G. (1969). On the mechanism of Langmuir circulations and their role in epilimnion mixing. *Limnology and Oceanography*, 493-503

Scott, W.E. (1991). Occurrence and significance of toxic cyanobacteria in southern Africa. *Water Science and Technology, 23*, 175-180

Shi, W., & Wang, M. (2009). An assessment of the black ocean pixel assumption for MODIS SWIR bands. *Remote Sensing of Environment, 113*, 1587-1597

Simis, S.G.H., Peters, S.W.M., & Gons, H.J. (2005). Remote sensing of the cyanobacterial pigment phycocyanin in turbid inland water. *Limnology and Oceanography, 50*, 237-245

Simis, S.G.H., Ruiz-Verdu, A., Dominguez-Gomez, J.A., Pena-Martinez, R., Peters, S.W.M., & Gons, H.J. (2007). Influence of phytoplankton pigment composition on remote sensing of cyanobacterial biomass. *Remote Sensing of Environment, 106*, 414-427

Southern Waters Ecological Research and Consulting. (2000). Zeekoevlei/Rondevlei rehabilitation study: final report. *DH Environmental Consulting, 1*, Cape Town

Stramski, D., Bricaud, A., & Morel, A. (2001). Modeling the inherent optical properties of the ocean based on the detailed composition of the planktonic community. *Applied Optics, 40*, 2929–2945

Vermote, E.F., Tanre, D., Deuze, J.L., Herman, M., & Morcette, J.J. (1997). Second Simulation of the Satellite Signal in the Solar Spectrum, 6S: an overview. *Geoscience and Remote Sensing, IEEE Transactions on, 35*, 675-686

Vidot, J., & Santer, R. (2005). Atmospheric correction for inland waters-application to SeaWiFS. *International Journal of Remote Sensing, 26*, 3663-3682

Walters, N.M., Kok, C.J., & Claase, C. (1985). Optical properties of the South African marine environment. In L.V. Shannon (Ed.), *South African ocean colour and upwelling experiment* (pp. 157). Cape Town, South Africa: Sea Fisheries Research Institute

Yacobi, Y.Z., Gitelson, A., & Mayo, M. (1995). Remote sensing of chlorophyll in Lake Kinneret using highspectral-resolution radiometer and Landsat TM: spectral features of reflectance and algorithm development. *Journal of Plankton Research, 17*, 2155-2173

Zimba, P.V., & Gitelson, A. (2006). Remote estimation of chlorophyll concentration in hyper-eutrophic aquatic systems: Model tuning and accuracy optimization. *Aquaculture, 256*, 272-286

1